PREPARATION OF CLAY-COATED GLASS SURFACES FOR MICROFLUIDICS-BASED STUDY ON CLAY-FLUID INTERACTIONS

By

RUPOM BHATTACHERJEE

Bachelor of Science in Petroleum & Mining Engineering

Shahjalal University of Science & Technology

Sylhet, Bangladesh

2017

Submitted to the Faculty of the
Graduate College of the
Oklahoma State University
in partial fulfillment of
the requirements for
the Degree of
MASTER OF SCIENCE
July, 2021

PREPARATION OF CLAY-COATED GLASS SURFACES FOR MICROFLUIDICS-BASED STUDY ON CLAY-FLUID INTERACTIONS

Thesis Approved:

Dr. Prem Bikkina

Thesis Adviser

Dr. Javier Vilcaez

Dr. Mohammed Al Dushaishi

ACKNOWLEDGEMENTS

I owe an expression of gratitude to the people who have supported me throughout the study. Without their support and encouragement, the quality of this thesis would have inevitably suffered.

First of all, I wish to deliver my deep respect and gratefulness to my advisor and the chair of my committee, Dr. Prem Bikkina, for his constant guidance, technical and intellectual contribution in every step of this study. From conducting the experiments to writing the thesis, Dr. Bikkina diligently shared his expertise and knowledge to make the thesis more meaningful and effective.

I would also like to extend my sincere thanks to my committee members Professor Dr. Javier Vilcaez and Dr. Mohammed Al Dushaishi, for their advice and suggestions in general.

I would forever be grateful to Professor Dr. Jim Puckette for helping me prepare the clay samples. I also thank professor Dr. Josh Ramsey and his student Saeed Manouchehri for helping me with the Zeta Potential measurement, Dr. Geir Hareland and his student Nicolai Kjeldal for the fluid rheology measurement, Brent Johnson and Lisa Whitworth from the Microscopy Lab of OSU for their technical support in the microscopic analysis, my colleague Sushobhan Pradhan, and Imran Shaik for helping me on fittings and providing suggestions many times during the experiments.

Finally, I express my gratitude to DOE and Continental Resources (Award Number: DE-FE0031776) for funding this study and the PI of this project, Professor Dr. Mileva Radonjic, for her amiable support and continuous encouragement.

Name: RUPOM BHATTACHERJEE

Date of Degree: JULY, 2021

Title of Study: PREPARATION OF CLAY-COATED GLASS SURFACES FOR MICROFLUIDICS-BASED STUDY ON CLAY-FLUID INTERACTIONS

Major Field: PETROLEUM ENGINEERING

Abstract: Unique characteristics of clay, even though make any clay abundant shales a good source of adsorbed gas, make them equally difficult to produce. The clay-water interaction can cause significant swelling and fines migration in the shale formation, both of which can significantly impair the overall hydrocarbon recovery from shale.

Geomaterial micromodels, developed by functionalizing traditional glass or PDMS surface with geomaterials (e.g., calcite, quartz, clay) can represent the physico-chemical properties of the natural porous media and have been used during the last few years to understand and evaluate the solid-fluid physicochemical interactions. This study focuses on developing a clay-coated geomaterial surface and investigates the effect of base fluid's salinity on clay adsorption to the glass surface. Glass capillary tubes and straight channel borosilicate glass micromodels are coated with Illite clay minerals to represent the pore-scale clay chemistry of Caney Shale, a Mississippian unconventional play in Southern Oklahoma, USA. 10 wt. % of Illite clay slurries made with brines of four different salinities are used to coat the glass-capillary tubes to understand the effect of salinity in clay adsorption on the glass surface and overall coating quality. To achieve a stable coating and evaluate the impact of heat treatment on coating's stability, straight channel glass flow cells coated with Illite clay are heat-treated at low (25 °C) and high temperature (125 °C). Dynamic flooding tests were carried out with brines on the coated surface to evaluate the stability of the coating.

The experiments' outcome indicated a strong relationship between the brine's salinity and the adsorption of clay particles on the glass surface. An increase in brine concentration resulted in improved adsorption of clay particles on the glass surface. Experiments involving heat treating the glass surface following the coating demonstrated significant improvement in the stability of the coating.

TABLE OF CONTENTS

Chapter Page

LIST OF TABLES

Table Page

LIST OF FIGURES

Figure Page

CHAPTER I

INTRODUCTION

Clay minerals account for, on average, 60 wt.% of most shales [1]. It is generally agreed that the presence of clay can significantly affect the fluid flow through the low permeable porous media. This effect is mainly due to the swelling induced in clay as a result of the interaction between injected water-based fluids and clay minerals, resulting in reduced pore space and permeability [2, 3].

Different clay minerals have different levels of swelling potential depending on their structural composition and cation exchange capacity (CEC). For example, Smectite and Illite having surface area and CEC larger than other common clay minerals, such as Kaolinite and Chlorite, demonstrate greater affinity to adsorb water into the formation causing significant swelling in the rock matrix [4].

Shales' productivity can also be affected by fines migration. Release of the clay particles upon exposure to low salinity injection fluids can clog the narrow pore throats and damage the formation permeability [5]. Thus, through fines migration, even the non-swelling clays such as Kaolinite and Chlorite might as well affect the formation permeability.

Different laboratory tests-, such as dispersion test, immersion test, bulk hardness test, etc. are developed to study the fluid interaction with shale rock. [6]. However, these tests are designed to

assess the rock samples' stability by immersing them in fluids [7] or flowing the fluids through the sample [8, 9]. Since rocks are usually composed of more than one mineral (quartz, calcite, clay, etc.), these tests can not recognize the potential clay-fluid interaction and its impact on formation damage. Moreover, these tests' results do not reflect the in-situ behavior of clay upon exposure to any fluids.

Geomaterial functionalized microfluidic chip, developed by coating traditional transparent micromodels with any geomaterials, is an excellent tool that can be facilitated with the required level of surface heterogeneity and surface chemistry to represent the pore-scale flow dynamics. Geomaterial microfluidics provides the ability to mimic specific surface mineralogy of any rock and visually study the surface's behavior upon exposure to any fluid. Besides, the micromodel flow networks are highly customizable and provide flexibility in chip design as well as easy and accurate control of fluid flow.

Microfluidics has been used extensively during the last few years to understand and evaluate solid-fluid physicochemical interactions [5, 10-19]. Precisely two different methods have been developed to functionalize the traditional glass or PDMS micromodels with clay minerals: physical adsorption by flowing clay slurry through the flow network [12, 20] and layer by layer deposition of polyelectrolyte and clay [21]. Song and Kovscek (2015, 2016) functionalized a silicon microfluidic chip with Kaolinite clay by injecting a clay solution of 1 wt.% of Kaolinite clay in 15,000 ppm NaCl brine to study the effect of low salinity water flooding in sandstone reservoirs [5, 20]. Following the coating, they exposed the surface to120 °C for 25 minutes to create an immobile clay surface and study the wettability alteration due to clay adsorption. A similar approach was followed by Amirian et al. (2017, 2018) to develop Kaolinite [12] and Illite [11] coated geomaterial surface to understand the effect of clay type and water composition on low salinity water flooding. They used a 20 wt.% of clay slurry made of 30000 ppm of NaCl brine, and instead of heat drying the coated surface, they air-dried it for two hours by placing it on a hot plate at 80 °C to ensure the

reversibility of the coating. Barnaji et al. (2016), instead of using any brine for base fluid, used a suspension of 10 wt.% of clay in distilled water to coat the glass surfaces with Kaolinite and Sodium Bentonite clay and dried the micromodel by placing it in an oven at 120 °C for 1 hour [22]. Mahani et al. (2015, 2017) used deionized water and Isopropyl Alcohol (IPA) to prepare a Na-Montmorillonite clay suspension before depositing on a dried glass substrate and a glass micromodel, respectively [23]. Following the deposition, they vacuum dried the glass substrates at a temperature of 60°C.

As it can be seen, there is not a good agreement between the works of literature on the specification (e.g., salinity) of the base fluid used to make the clay suspension. Furthermore, the post-coating treatment to achieve a stable coating also varies widely in the literature. However, as per the DLVO (named after Boris Derjaguin and Lev Landau, Evert Verwey, and Theodoor Overbeek) theory, the presence or absence of cations in the carrier fluid is critical for the attachment or detachment of clay particles from the rock surface [14, 24]. Given the advantages of using geomaterial micromodels to study clay-fluid interaction to unearth the true potential of unconventional rocks, it is imperative to evaluate the effect of base fluid's salinity and drying treatments on clay adsorption to the glass surface and the stability of the coating, respectively. This will help reach a consensus over the solution preparation and drying procedure required for a successful clay coating.

This thesis focuses on developing a clay-coated borosilicate geomaterial micromodel to study phenomena such as formation damage, fines migration, and wettability alteration caused by clay upon exposure to different injection fluids. Illite, the dominant clay mineral of the Caney formation of Southern Oklahoma, USA, is used to coat the resealable borosilicate straight channels so that the developed geomaterial surface will be able to represent the pore-scale clay chemistry of the Caney shale.

The effect of the salinity of base fluid on the adsorption of the clay particles to the glass surface is evaluated by coating borosilicate glass capillary tubes with Illite clay slurries made with brines of four different salinities. In addition, to assess the effect of heat-treatment on the stability of the adsorbed clay particles, clay-coated surfaces are dried at two different temperatures, 25 ℃ and 125°C, and then exposed to brines of varying salinities.

This work can be helpful to reach a consensus over the solution preparation and drying techniques necessary to develop a clay-coated geomaterial surface. The developed Illite coated glass surface will be helpful to directly visualize the behavior of clay upon exposure to water-based drilling and fracking fluids and quantify the degree of swelling and fines migration. Experiments with brines of different salinities will be helpful to understand the effect of salinity on the adsorption of clay particles on the glass surface. The major applications include studying enhanced oil recovery in clay-rich formations and designing injection fluids to improve production from clay-rich unconventional formations without compromising the formation permeability.

A brief outline of this study is as follows: A comprehensive literature review on clay chemistry, its effect on shale rocks' productivity, microfluidics, and visualization techniques employed in this study is provided in chapter 2. Chapter 3 describes the materials and methods utilized to prepare the clay-coated surface and study the effect of salinity and heat treatment. Chapter 4 shows the results obtained from the study and discusses them. Finally, the conclusion and recommendations for future work are discussed in chapter 5.

CHAPTER II

REVIEW OF LITERATURE

2.1 Clay Fundamentals: A Brief Introduction

Clay is an earthy material composed primarily of very fine-grained (grain size < 4μm) clay minerals and traces of quartz (SiO_2), metal oxides (Al_2O_3, MgO, etc.), and organic matter. Clay minerals are known as phyllosilicates containing two fundamental crystal sheets: tetrahedral silica and octahedral alumina or magnesia. Millions of these single tetrahedrons and octahedrons get connected with each other in two directions and form the foundation of clay structures. Clays are generally plastic at appropriate water contents and solidify when dried [25].

Based on the proportion of the sheet, clays are classified as 1:1 (e.g., Kaolinite) and 2:1 (e.g., Illite, Smectite, Chlorite) phyllosilicates. Figure 1 is showing the structures of a single silicon tetrahedron and a single aluminum octahedron.

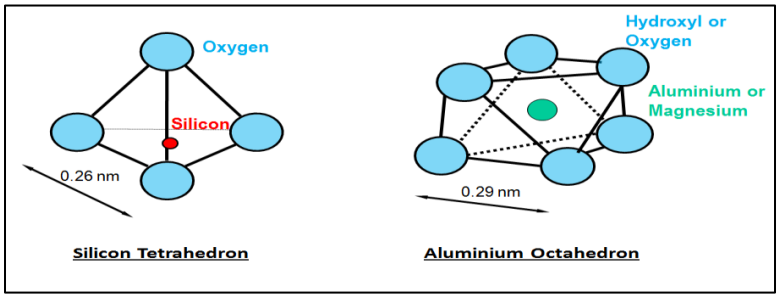

Figure 1: Basic structural units of clay minerals [26]

A silica tetrahedron (SiO_4) is formed when one silicon atom is connected with four oxygen atoms. Each SiO_4 tetrahedron shares three oxygen atoms with others and thus forms two-dimensional sheets. An alumina unit is formed by connecting one aluminum atom with six oxygen or hydroxyl atoms. Each hydroxyl ion is connected with three alumina units when forming an octahedral alumina sheet.

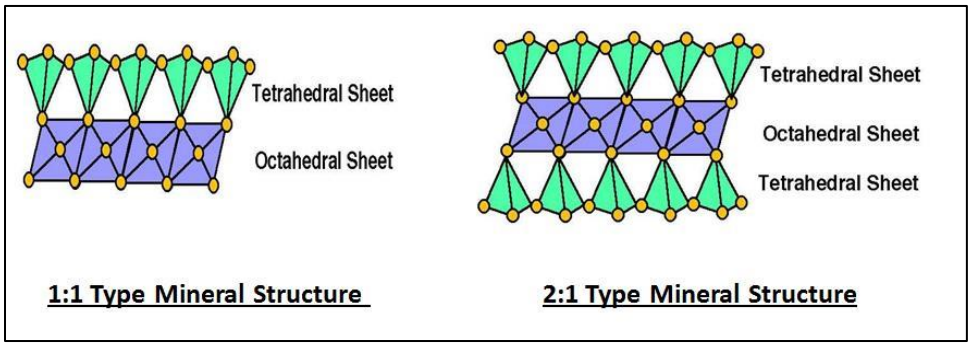

Figure 2: Structure of 1:1 Type clay minerals (e.g., Kaolinite, Halloysite) and 2:1 Type clay minerals (e.g., Illite, Smectite) [26]

Clay minerals are subjected to isomorphic substitution (replacement of cations in tetrahedrons or octahedrons), where Al often replaces Si in the tetrahedrons, and Mg replaces Al in octahedrons. This type of substitution by lower valance cation creates a deficiency of positive charges inside the crystal and makes the clay negatively charged. Besides, depending on the pH of the environment, the broken edges (Al−OH or Si−OH) of the 2:1 clay mineral can possess variable charges [27].

Kaolinite is a 1:1 silicate mineral where one tetrahedral unit is linked through an oxygen atom with another octahedral unit (Fig. 2). Because each tetrahedron-octahedron layer (T-O) in Kaolinite is connected with Van der Waals force and strong hydrogen bond, Kaolinite is a non-swelling clay. On the other hand, Illite is a 2:1 clay mineral where one octahedral sheet is sandwiched between two tetrahedral sheets (T-O-T). They have potassium ions between the layers, prevent water from encroaching the interlayer region. That is why Illite is less sensitive to swelling. However, in the case of Smectite, each T-O-T layer is connected with another T-O-T layer with a weak Van der

Waals force. Therefore, water can easily encroach between the layers, making Smectite a highly expandable clay.

Clay materials can also be composed of more than one clay mineral, and the mixture or interstratification of multiple clay minerals can be of different types such as ordered, segregated order, or even random (Fig. 3) [28, 29]. Some commonly found mixed-layer clay minerals include Illite-Vermiculite, Illite-smectite, Chlorite-Smectite, and Kaolinite-Smectite. Dissolution/recrystallization and the transformation of one mineral to another due to weathering (e.g., removal or uptake of cations, hydrothermal alteration, removal of hydroxide interlayers, etc.) are mainly responsible for the formation of mixed-layer clays [28-30]. For example, Smectites alter to Kaolinite via mixed layer Kaolinite/Smectite due to weathering. Likewise, Illite, Chlorite, and Micas transform to Vermiculite and then Smectite via mixed layer clays involving Vermiculite and Smectite [31].

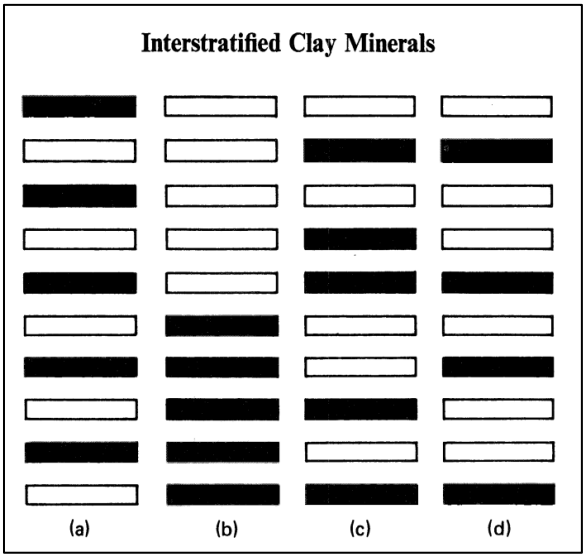

Figure 3: Types of mixed layering of clay minerals: (a) alternating; (b) segregated; (c) random; (d) general that includes more than one type of stratification. The rectangular boxes represent the individual component layer [28]

2.2 Influence of Clay on Shale Rocks' Producibility

Nowadays, most of the drilled formations in the USA are shales, and clay minerals constitute a significant portion of the shale rock's composition (Fig. 4). Clay influences oil and gas production from shale reservoirs in several ways. The high surface area of clays contributes to increased gas adsorption but negatively affects the permeability of the rock. Permeability is also compromised when swelling and fines migration are induced in the formation due to clay-water interaction. Besides, clay can alter the wettability of the rock from water-wet to oil-wet and affect the hydrocarbon displacement from the porous media. The following three sections briefly describe the effect of high surface area, swelling, and fines migration on shale's hydrocarbon productivity.

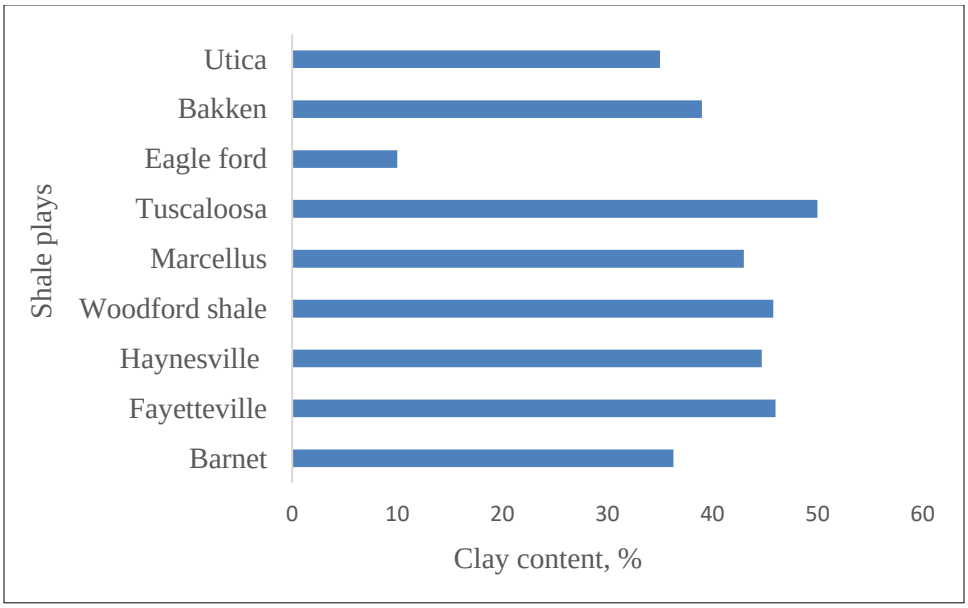

Figure 4: Average clay content in US Shales [32]

2.2.1 Effect of High Surface Area

The amount of adsorbed gas in a shale play increases as the surface area increases. Because of their platy structure, clay minerals are associated with large surface areas (Fig. 5). This increased area, even though helps a considerable amount of gas to be adsorbed on the shale rock surface, may create additional problems for fluid flow through the formation. According to Kozeny's equation,

permeability is inversely proportional to the square of specific surface area if the grain shape effect is ignored [33]. That means formations with higher surface area will have lower permeability. Therefore, formations with similar porosity may have different permeability if the clay content is different.

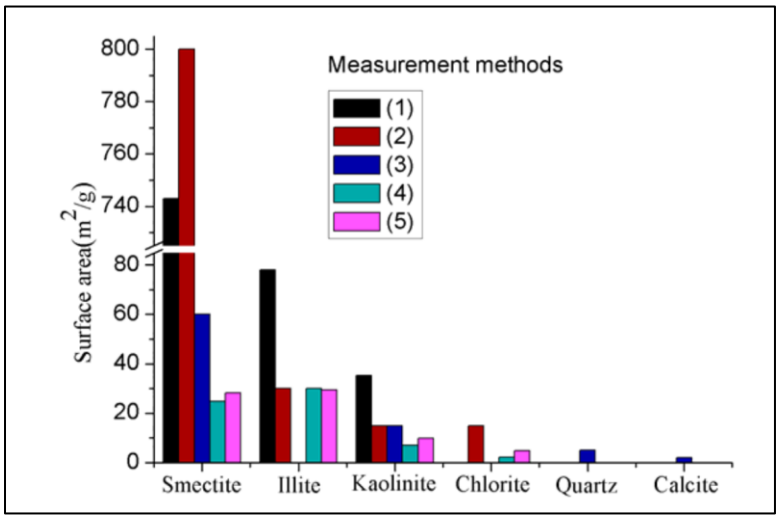

Figure 5: Surface areas of various clays and some other major minerals in rock measured using (1) Methylene blue absorption (2) Adsorption of water (3)Extrapolation from N_2 BET (4) N_2 BET surface area (5) CO_2 equivalent surface area [32]

2.2.2 Cation Exchange Capacity

As discussed in section 2.1, clays have a net negative charge on them because of their structure. To maintain electrical neutrality, they attract counter-ions from their surroundings. These ions are hydrated, have a shell of water surrounding them, and are exchangeable with other cations. Cation exchange capacity (CEC) is the total capacity of clay to hold the exchangeable cations. In another sense, it is just the reactivity of any particular clay.

Clays with higher CEC tend to have a higher negative charge and need more positive hydrated ions. Different clay minerals have different CECs depending on their structural charges and isomorphic substitution. Clays with higher CEC have a stronger attraction to water molecules.

Table 1: Cation exchange capacity (CEC) of some common clay minerals [34]

Clay Mineral	CEC (mEq/100g)
Kaolinite	3-15
Halloysite	5-50
Illite	10-40
Chlorite	10-40
Smectite	60-150
Vermiculite	100-150

2.2.3 Clay Swelling

Clay Swelling is a common phenomenon, happens when certain types of clay minerals come in contact with water-based fluids. Depending on the mechanism of water encroachment, there are two types of clay swelling that might occur: (1) crystalline swelling and (2) osmotic or double-layer swelling. Crystalline swelling occurs due to the adsorption of water molecules on the interlayer space between 10-22 Å. The primary mechanism behind crystalline swelling is the hydration of cations presented on the interlayer region and depends on the hydration energy of the cations. Usually, Na-montmorillonites are more prone to crystalline swelling than Mg or Ca-montmorillonite because Na has higher hydration energy than Mg or Ca. This type of swelling can happen to any 2:1 clay mineral and lead to a stepwise increase of the basal spacing. Osmotic swelling, on the other hand, happens due to the increase in double-layer spacing between clay molecules when they encounter brines of less salinity. It depends on the charge and cation exchange capacity of clay minerals. Usually, smectites are highly prone to osmotic swelling, for they have a net negative charge of -2 and a significantly high cation exchange capacity (Table 1). Unlike crystalline swelling, osmotic swelling leads to a continuous increase in basal spacing.

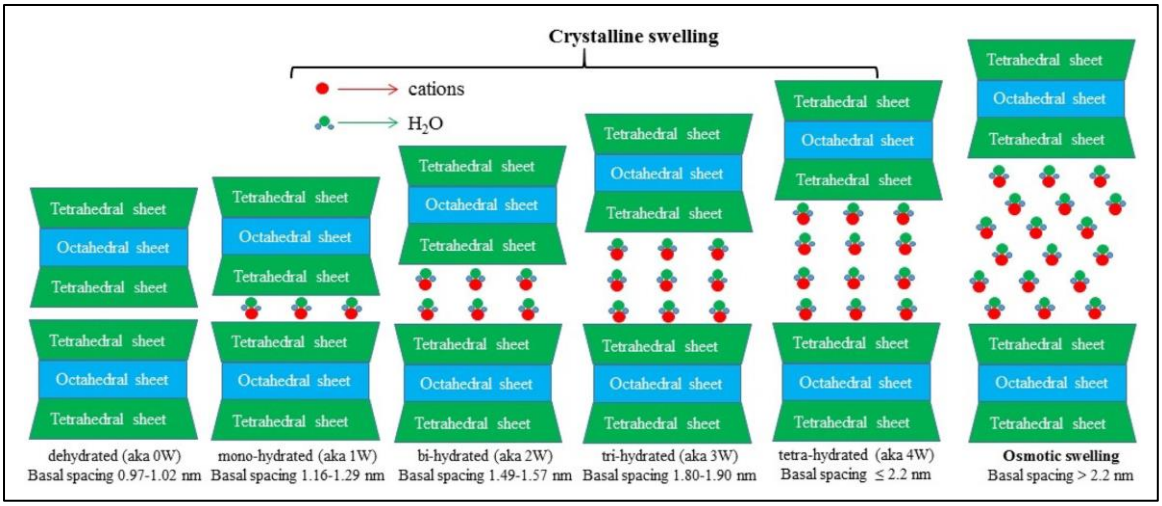

Figure 6: Schematic diagram of different types of swelling in expansive clays [35]

Regardless of the type, clay swelling significantly affects the permeability of the shale reservoir as it not only limits the size of the pore space and pore throat required for hydrocarbon movement in the shale matrix but also compresses and closes the created fractures, and therefore eventually limits the productivity of the shale formation. The most significant swelling-induced permeability reduction is created when clay minerals interact with fresh water [36].

2.2.4 Effect of Fines Migration

Fines migration is another feature of clay particles that has a considerable impact on shale's hydrocarbon productivity. The formation water being saline achieves an equilibrium condition with the clay minerals, which is disturbed when the formation water is replaced by injected water or any water-based fluid. When the injected fluid is less saline than the formation water, the deficiency in the counter-ions causes the expansion of the electrical double layer of the clay particles. This increases the double layer repulsive forces between the particles and causes the release of clay particles in the pore space. This phenomenon is known as fines migration, and the released fine can clog the narrow pore throats and affect the formation permeability.

Figure 7 shows the change in double-layer spacing (D-spacing) of different clay minerals with different brine concentrations. The D-spacing is increasing with the decrease in brine concentration regardless of the type of clay minerals. However, there is a certain concentration of brine, known as critical brine concentration, which is needed to supply enough counter-ions to prevent the increase in D-spacing and the migration of fines. Here, in this case, when the brine concentration was higher than 0.5 M, the double layer spacing became almost zero. Therefore, in this case, 0.5 M is the critical brine concentration needed to prevent the fines migration.

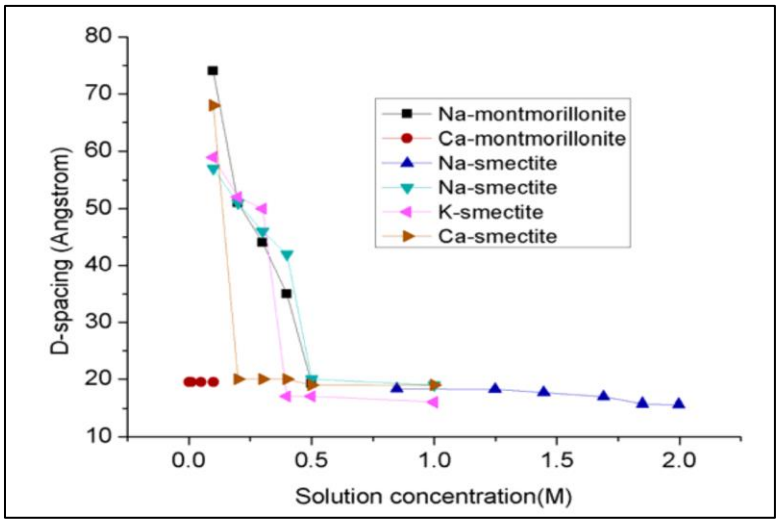

Figure 7: The double-layer spacing of clay minerals in brine solutions of different concentrations [3, 21, 37, 38]

2.3 Caney Shale Clay Mineralogy

This study focuses on developing a clay-coated geomaterial surface representing the clay chemistry of the Caney shale of southern Oklahoma, USA. Caney, an emerging unconventional formation, is located in the southern mid-continent Anadarko, Ardmore, Marietta, and Arkoma basin [39-41]. The formation is 60 to 300 meters thick, rich in total organic carbon (0.5 to 11%), and a part of South Central Oklahoma Oil Province (SCOOP). Caney is Mississippian in age, sits on top of the Woodford shale- the primary oil-bearing formation in this region, and has extensive oil and gas resources [39].

Caney Shale
"Mayes" Formation

Richardson 2-33

Sample	CLAYS				CARBONATES			OTHER MINERALS					SUM		
Depth (ft)	Chlorite	Kaolinite	Illite	Mx I/S*	Calcite[1]	Dol/Ank**	Siderite	Quartz	K-spar	Plag.	Pyrite	Apatite	Clays	Carbonates	Other Minerals
5908.0	4	3	13	1	1	trc	2	61	1	3	1	10	21	3	76
5927.0	2	7	29	2	1	1	3	33	2	5	2	13	40	5	55
5996.0	3	4	20	9	28	4	0	27	1	2	2	0	36	32	32
6142.0	1	0	3	trc	14	66	Tr	11	2	3	trc	Tr	4	80	16
6208.0	1	1	14	3	14	7	Tr	50	3	6	trc	1	19	21	60

Rogers Trust 1-24

Sample	CLAYS				CARBONATES			OTHER MINERALS					SUM		
Depth (ft)	Chlorite	Kaolinite	Illite	Mx IS*	Calcite[1]	Dol/Ank**	Siderite	Quartz	K-spar	Plag.	Pyrite	Apatite	Clays	Carbonates	Other Minerals
6778.00	trc	10	16	18	4	5	0	31	1	4	2	9	44	9	47
6826.00	trc	6	19	16	10	2	0	36	0	5	4	2	41	12	47
6846.00	4	trc	22	25	13	3	0	25	trc	4	4	trc	51	16	33
7059.00	0	0	17	4	12	21	0	40	trc	3	3	trc	21	33	46

*Ordered interstratified mixed-layer illite/smectite, with 35% expandable interlayers for samples with abundant mixed-layers
**Includes dolomite and iron-bearing dolomites (i.e., Fe-dolomite and ankerite
***No mixed illite, all smectite
[1]Includes the Fe-rich varieties

Figure 8: Caney Mineralogy obtained from Sidewall Cores. The "Mayes" formation is a calcareous shale deposit found at the base of the Caney Shale [41]

However, the development of this shale has been impeded by clay and the reactivity of clay with water-based fluids. X-ray Diffraction (XRD) data on several Caney core samples from different depths indicated that the clay mineralogy of Caney is dominated by Illite [39, 41, 42]. Even though there exists some Illite-Smectite mixed clay, the contribution of Illite outnumbers Smectite.

2.4 Background of Microfluidics

Microfluidics, a generic term referring to the fluid phenomena at small channels with dimensions of tens to hundreds of micrometers, is the study of fluid in a geometrically constrained environment where the flow is controlled by surface forces rather than volumetric [43]. In general, microfluidic chips (micromodels) are made of transparent materials such as glass, polydimethylsiloxane (PDMS), polystyrene, polycarbonate, etc. Irrespective of the material used, micromodels allow direct visualizations of the flow networks created by etching the micromodel material based on a predesigned geometric shape, thus allowing a highly customizable flow network. Details on the micromodel fabrication are provided by Amirian T. (2019) [10].

Microfluidics emerged at the beginning of the 1980s and potentially influenced different subject areas such as physics, chemistry, biochemistry, and biotechnology [44]. In recent years microfluidics has started gaining acceptance in petroleum fields precisely to study multiphase flow through porous media [13, 18, 45]. The use of these chips to study flow through porous media is advantageous. It provides the ability to visually study the fluid flow and the effect of surface and interfacial forces. Moreover, the flow network in micromodel is highly customizable, can be designed to represent complex rock networks found in physical rocks.

2.4.1 Geomaterial Micromodel

Traditional glass or PDMS micromodels even though represent the subsurface flow network through a successful microfabrication, cannot be accounted for the unique surface chemistry associated with different types of rock. The glass micromodels, to some extent, can be used to study

the fluid flow in sandstone rocks as the primary constituent for both of these substrates is silica. However, other significant hydrocarbons bearing rocks such as carbonates (e.g., limestone and dolomite) and shales have utterly different types of mineralogy, hence cannot be represented by any traditional off the shelf micromodels. Carbonates are formed mainly of Calcite or Aragonite-two different crystal forms of $CaCO_3$, while shales are mostly clay-rich formations. Clays themselves are composed of different clay minerals, and their behaviors upon exposure to fluids are also different, as discussed in section 3.1 and section 3.2.

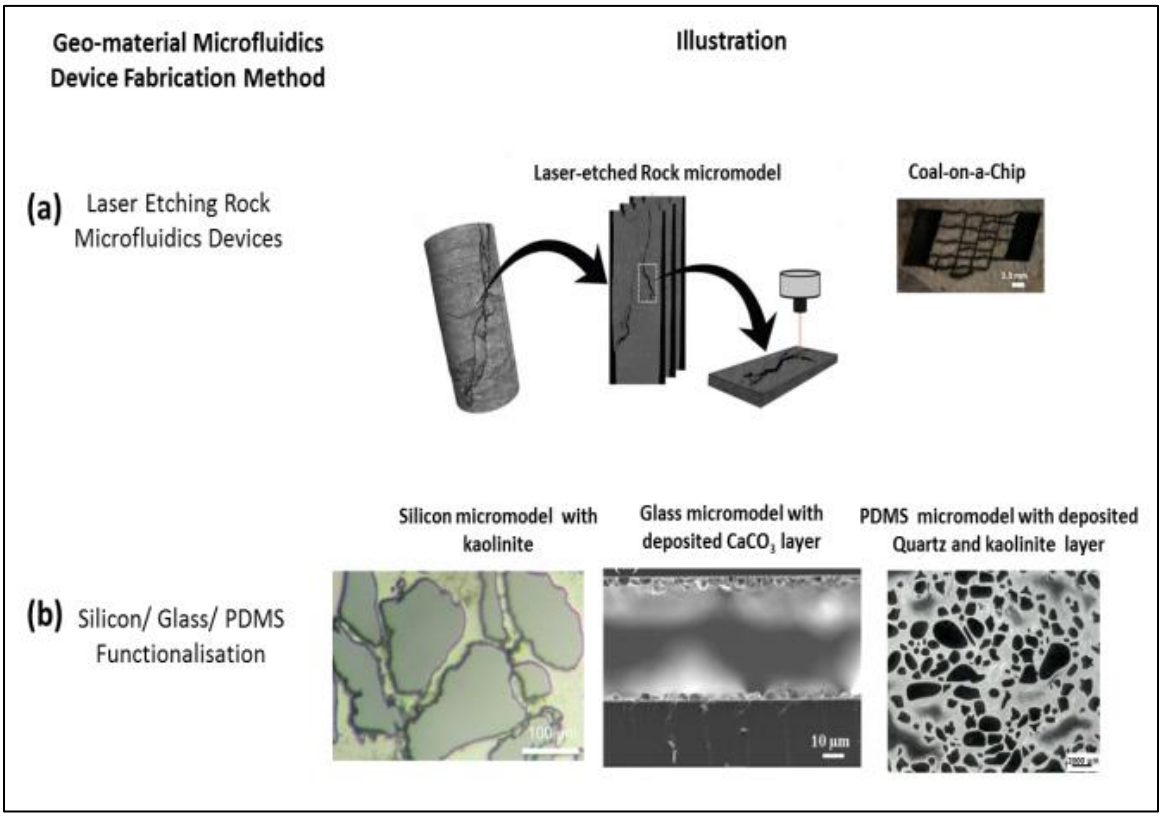

Figure 9: Different fabrication methods of developing geomaterial micromodel [10, 20, 46]

The limitation of traditional glass micromodels of appropriately representing the solid substrate can be lessened by using geomaterial micromodels developed either by laser-etching real-rock samples or by functionalizing traditional micromodels with geomaterials such as coal, calcite, clay, etc. For example, Gerami et al. (2017) developed a coal micromodel by etching fracture on an actual coal

surface to compare the micro-fracture geometry with coal cleats and visualize fluid transport in coal micromodel [46]. Laser micromachining was used to etch the coal surface and PDMS to seal the etched fractures along the top surface of the geomaterial micromodel. They observed higher roughness on the fabricated micromodel when it is prepared by cutting the coal sample parallel to the bedding plane. The dynamic contact angle in the micromodel was also found to be very heterogenous as the real coal sample. In an attempt to use microfluidics to study carbonate rocks, Wang et al. (2017) developed a geomaterial micromodel that can represent a limestone reservoir. They coated a glass micromodel with $CaCO_3$ nanocrystal by adding a silane agent, Ca^{2+}, and CO_3^{2-} ions and allowing the calcite crystals to grow in situ on the glass surface [47]. They incorporated their model to visualize water-oil-carbonate real-time interactions with fluorescence microscopic imaging. A similar method was used by Shaik et al. (2020) to develop calcite-coated glass capillary tubes and micromodels. The substrates were used to understand the effect of cleaning, silane agent, and supersaturation on $CaCO_3$ deposition on the glass surfaces.

To prepare clay-coated micromodels, Song and Kovescek (2015) developed a method of functionalizing silicon micromodel with Kaolinite clay by injecting Kaolinite suspension into the micromodels. After coating, they dried the micromodel by flowing air through it to prepare a reversible coating and keeping it in an oven at 120 °C for 25 minutes to prepare the irreversible one. The reversible one was used to study the migration of clay particles when exposed to low salinity water flooding, whereas the irreversible one was used to study wettability alteration in sandstone reservoirs owing to the presence of clay. A similar approach was adopted by Amirian et al. (2017) to develop Illite and Kaolinite coated geomaterial surfaces. Following the coating, they air-dried their micromodel at 80 °C for 2 hours to have a reversible layer of clay particles on the glass surface, which they used to study the mechanism of low salinity water flooding in sandstone reservoirs [12]. Different from the above-mentioned clay coating procedure, where the clay particles get physically adsorbed into the substrate surface- very similar to how natural deposits of clay form- a layer-by-layer method of clay coating was developed by Zhang et al. (2018) to

functionalize glass and PDMS micromodels with Kaolinite and Montmorillonite types of clay minerals. The layer-by-layer deposition method involved injecting PDDA- Poly (diallyldimethylammonium chloride) solution to link the substrate surface and clay minerals [21]. They used static and dynamic flooding of brines to assess the stability of the coated surface and reported the coating to be more stable than that can be achieved by mere injection of clay solution through the micromodels.

2.5 Measurements and Visualization Techniques

2.5.1 Optical Microscopy

Optical microscopes, often known as light microscopes, are an elementary form of microscope that usually employ a camera, objective lenses, stage, eyepiece, condenser, and light source to magnify and generate a magnified image of any object. The condenser collects the light from the light source and directs the light to the specimen placed on the stage right below the objectives. The objective collects the light passing to the specimen, and the eyepiece creates the magnified image.

Depending on how the microscope gets light to the objective lens, optical microscopes are divided into transmitted and reflected light microscopy. In transmitted microscopy, the light source is placed below the specimen, and light transmits through the specimen to the objective. This kind of microscopy is helpful to distinguish the morphological properties of the specimen that is transparent or semi-transparent. Reflected-light microscopy, where the light source is usually placed above the specimen and is reflected from the specimen to the object, is typically used to examine thick and opaque specimens.

2.5.2 Scanning Electron Microscopy

Scanning Electron Microscope (SEM) is a type of electron microscope that emits electron beams to a specimen surface. As the surface gets hit by the beams, the electron interacts with the atoms, and the beams get bounced off. A detector registers those scattered beams and turns them into a

picture containing useful information about the surface topography and composition of the specimen. For SEM analysis, the specimen surface needs to be conductive. Usually, surfaces are coated with gold or carbon to make them conductive prior to the analysis.

2.5.3 Energy-Dispersive X-ray Spectroscopy

Energy-dispersive X-ray spectroscopy, or EDS, is an analytical technique used in combination with SEM to determine the presence of different chemical elements on the specimen surface and obtain the elemental map. In this technique, an electron beam with an energy level of 10-20 keV strikes the sample's surface and causes the emission of X-rays from the sample. Each element has a unique atomic structure causing distinguishable spikes in the X-ray emission spectrum; hence EDS-spectrum allows characterization of the elements [48].

2.5.4 Confocal Laser Scanning Microscopy

Confocal Laser Scanning Microscopy (CLSM) is a fluorescence microscopy technique that uses laser lines of different wavelengths to excite the sample surface. The fluorophores present in the sample adsorb the laser lights and cause detectable fluorescence. Fluorescent dyes are usually added to the samples if the samples are not inherently fluorescent. CLSM can eliminate any out-of-the-focus illumination and can be used to take images at different planes of focus. The surface can be divided into a number of slices based on the focus planes, and 2D images from each of the slices can be stacked together to make a 3-D image of the optical section of the sample. The 2-D and 3-D images can be helpful to understand the structure and provide insights into the appearance of the mineral coatings on any surface [49].

2.5.5 Atomic Force Microscopy

Atomic Force Microscopy (AFM) is a type of scanning probe microscopy that can be used to acquire high-resolution topographic images of almost any surface based on the interaction force between the surface and the sharp AFM tip mounted at the end of a cantilever. The AFM tip is equally sensitive in air and liquid environment. As the tip approaches the surface, the short-range attractive forces between the surface and the tip cause the cantilever to bend towards the surface. However, as the cantilever is brought closer, the repulsive forces cause the cantilever to bend away from the surface. A position-sensitive detector known as a photodiode is employed with the AFM that records the deflection of the cantilever via a laser beam that is reflected off the flat top of the cantilever (Fig. 9). Any bending in the cantilever will cause changes in the direction of the reflected beam. The roughness of the surface influences the deflection of the cantilever, and an actual topographic map of the surface is thus generated. When used with appropriate theory, the probe interaction with the sample surface can also be used to measure the surface charge of various materials, including clay minerals and rock [50, 51].

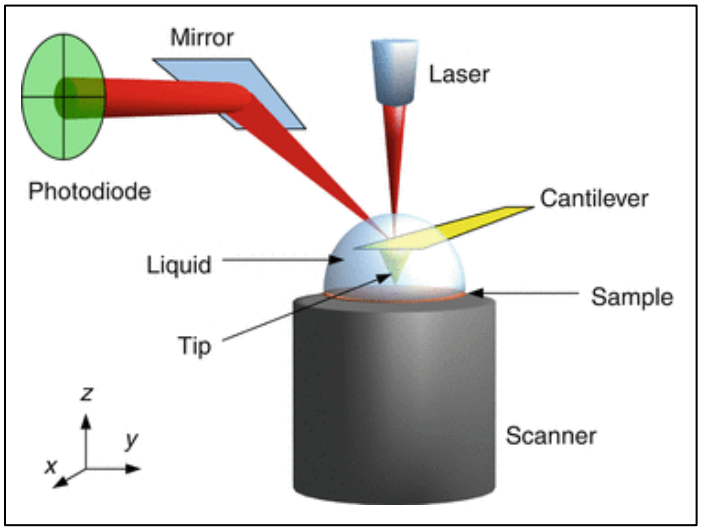

Figure 10: Schematic of AFM in liquids [52]

CHAPTER III

MATERIALS AND METHODS

3.1 Clay Minerals

Illite (IMt-1) from Silver Hill's Cambrian Shales, Jefferson Canyon, Montana, USA, supplied from the source clays repository of the Clay Minerals Society, was used to coat the glass capillary tubes. Prior to coating, the clay chips were powdered in a ball mill for less than five minutes. Tungsten canister and balls were used to grind the clay chips to avoid trace contamination of Fe or Al. To coat the straight channel glass micromodels, Illite clay powder (IMC) was purchased from Lotioncrafter Inc.

Figure 11: Illite clay powders

Illite, $(K, H_3O)(Al, Mg, Fe)_2(Si, Al)_4O_{10}[(OH)_2, H_2O]$, is a 2:1 clay mineral where one octahedral alumina sheet is sandwiched between two tetrahedral silica. They have potassium ions between each Tetrahedral-Octahedral-Tetrahedral (TOT) sequence making them less vulnerable to water encroachment.

The Illite IMt-1 sample had already been characterized by Köster (1996). He identified the chemical composition of the clay sample by X-Ray diffraction analysis of various size fractions of the clay sample [53]. The chemical composition of the Illite clay obtained from the EDS elemental analysis of the Illite powders is shown in Table 2.

Table 2: Major components of the Illite clay (IMt-1 and IMC) as observed in EDS elemental map

	Mass Norm. %	
Element	**IMt-1**	**IMC**
Oxygen	46.50	51.80
Silicon	23.00	12.38
Aluminum	14.62	7.73
Potassium	7.80	2.60
Iron	5.23	3.14
Magnesium	1.58	1.50
Calcium	0.72	20.36
Titanium	0.37	0.34
Sodium	0.06	0.17
Zinc	0.03	0.01
Phosphorus	0.02	0

3.2 Fluids

Clay slurries were prepared with NaCl brines of different concentrations specified in table 3. The brines were prepared by dissolving NaCl powders purchased from Sigma Aldrich in deionized water (18.2 MΩ-cm).

Table 3: Basic properties of the clay solutions

Illite Clay Slurry	Base Fluid	NaCl Concentration, ppm	Dynamic Viscosity of clay slurry, cp	Density of clay slurry, g/cm^3	pH of clay slurry
01	Di water	0	0.5	1.5	8
02	Brine 1	5000	1.1	1.6	8.5
03	Brine 2	10000	1.2	1.65	7.9
04	Brine 3	30000	1.5	1.75	8.4

3.3 Solid Substrates

3.3.1 Capillary tubes

Glass capillary tubes purchased from DWK Life Sciences Kimble (catalog no. 34505–99) were used to develop the coating procedure and study the effect of base fluid's salinity on the adsorption of clay particles to the glass surface. The capillary tubes are made of borosilicate glass, 90 mm long, and have an outer diameter of 1.2-1.5 mm and a wall thickness of 0.2 mm.

3.3.2 Micromodels

Straight channel resealable flow cells, purchased from Micronit Micro Technologies B.V, were used to prepare the geomaterial surface and study the effect of heat treatment on the stability of the clay coating (Fig. 12). Flow cells are composed of two separate layers. The bottom layer is a 700 µm thick plain glass slide, whereas the top layer is an 1100 µm thick glass slide with inlet and outlet ports enclosed by an elastomer. When the bottom and top layers are installed in the chip holder, the elastomer seals the top and bottom layer and defines the flow path. The flow path is about 40 mm long and has a hydraulic radius of 1.5 mm. One of the major advantages of these flow cells is that they are resealable, meaning that the top and bottom layer can be disintegrated, and the surface can directly be used for microscopic analysis.

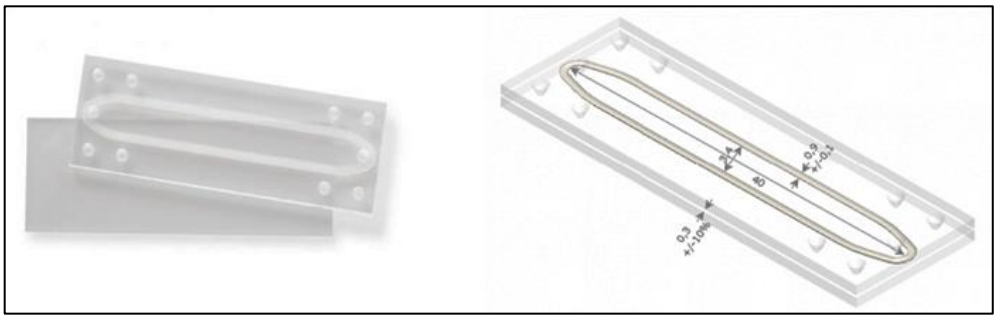

Figure 12: (left) Top and bottom part of resealable straight channel flow cell; (right) connected flow path with dimensions (Courtesy Micronit Microfluidics)

3.4 Syringe Pumps

One Standard Infuse/Withdraw PHD ULTRA™ Programmable Syringe Pump (figure 13), purchased from Harvard Apparatus, is used to transport the fluids back and forth to the capillary tubes and glass micromodels. The pump has the ability to flow the fluids continuously at a very low flow rate (1.56 pl/min using 0.5 µl syringe). The programmable feature allows automating the steps.

Figure 13: PHD Ultra Syringe Pump (Courtesy Harvard Apparatus)

3.5 Microscope, Camera, and Light Source

For microfluidic set-up, an integrated system of a 50MP 1080P 60FPS 4K camera mounted with a 0.7X-4.5X magnification C-mount lens was used to capture high-quality images of the glass

surfaces during and after coating. An LED-ring light source coupled with an adjustable 1.5-36 mm optical iris diaphragm was used to provide the illumination. The camera and the lens were purchased from Eakins Repair Tools, light source from Insein Li Fung Store, and iris from Walley Optics Store of AliExpress. Figure 14 shows the components of the microscopic system used in the microfluidics set-up, and figure 15 shows the system. The specifications of the components are shown in table 4.

Table 4: Specifications of the microscopy components used in the microfluidics system

Camera	Type: Digital HDMI/USB powered Picture pixel: 50MP Video frame rate: 4K@30FPS; 1920x1080@60FPS CMOS censer:1/2.33 inch CMOS pixel:1.55um x 1.55um
Lens	Type: C-mount lens Working distance: 95mm Adapter: 0.5X Barlow Lens (Increase working distance) Zoom ratio: 6.5:1 Objective magnification power: 0.7 - 4.5X Size: 168mm (L) * 50mm (D)
Light source	Type: Adjustable brightness LED bottom light source Outside Diameter: 90 mm Inside Diameter: 63 mm
Iris	Outside diameter: 56 mm Minimum aperture diameter: 1.5 mm Maximum aperture diameter: 36 mm Thickness: 6 mm Material: Metal Blades: 14 pieces

Figure 14: Components of the microscopic system used in the microfluidics set-up

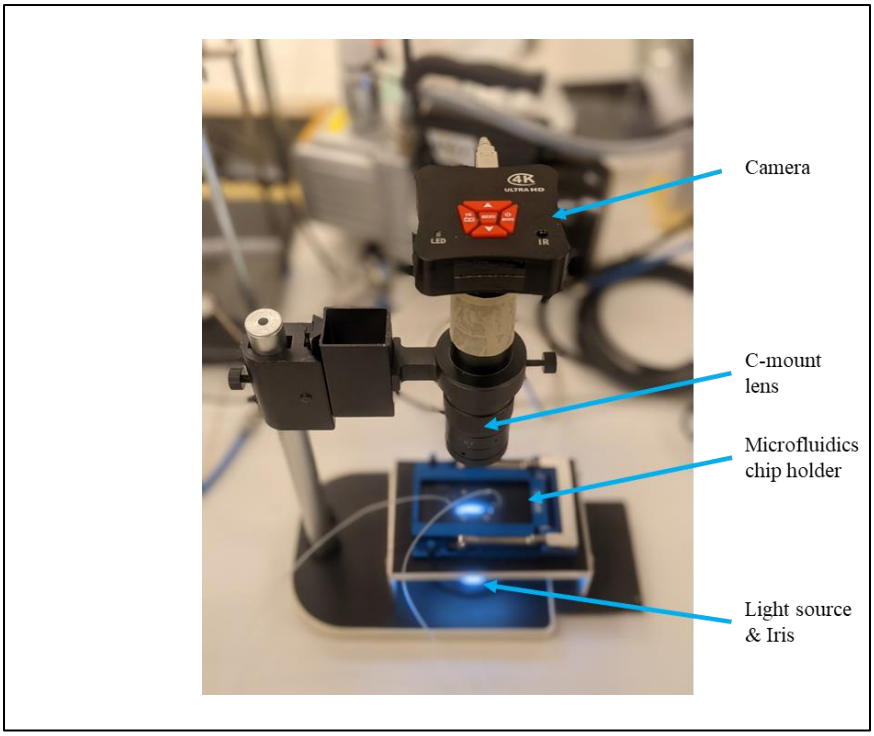

Figure 15: Microscopic system used in the microfluidics set-up

AmScope B250 binocular compound microscope and the built-in illumination system were used to take images of the coated capillary tube surfaces. SEM, SEM-EDS, and CLSM analysis of the coated surface was carried out in the Microscopic Laboratory of Oklahoma State University, USA using FEI Quanta 600 field-emission gun Environmental Scanning Electron Microscope, Bruker Energy-Dispersive X-ray Spectroscope, and Zeiss LSM 980 Airyscan 2, respectively. SEM and SEM-EDS were used for coating characterization described in section 3.7.3, while SEM and CLSM were employed to evaluate the stability of the coating explained in section 3.7.5.1. The specifications of the microscopes are listed in Table 4. Data are collected from Vendor's website [54] and Oklahoma State University's microscopy lab [55].

Table 5: Microscope specifications

Microscope	Specifications
AmScope B250	• Microscope Type: Compound • Magnification Power: 40X to 2500X • Objective Power: 4X, 10X, 40X, 100X • Eyepiece Power: 10X, 25X • Eyepiece Size: 23mm • Condenser: NA1.25 Abbe condenser with iris diaphragm • Condenser Type: Bright-field • Illumination: LED light, transmitted (bottom), intensity adjustable
FEI Quanta 600 Field-Emission Gun Environmental SEM with Bruker Energy-Dispersive X-Ray Spectroscope	• Resolution of 1.2 nm at 30 kV, 1.5 nm at low vacuum mode, and 1.5 nm at ESEM mode • Accelerating voltages up to 30 kV • Digital camera system • XFlash®6 detector series with active areas from 10 to 100 mm^2

Zeiss LSM 980 Airyscan 2	• Axio Observer 7 inverted microscope • Objectives: 10X, 20X, 40X water, 63X oil, and 100X oil objective lenses. • Lasers, all solid-state: 405, 445, 488, 514, 561nm, 639nm • Features: 2 photomultiplier tubes (PMTs), 32-channel spectral GaAsP Airyscan 2 detector, transmitted light PMT, motorized x-y stage, piezo z, temperature/CO2 incubation, ZEN Blue software.

3.6 Tubing, Valves, and Other Accessories

The tubing used to connect pumps and the microfluidics chip is FEP (Fluorinated ethylene propylene). They are transparent, have 0.25 mm inner diameter (ID), and 1.6 mm (1/16 ") outer diameter (OD). PEEK tubing (3.175 mm OD, 1.6 mm ID) was used to connect the syringe pump with the glass vial containing the clay solution. All these components were chemically compatible with aqueous and organic phase liquids used in these experiments. Swagelok three-way and two-way ball valves were used in this study.

Table 6: Tubing specifications

FEP Transparent Tubing	• Dimension: 1.16" OD x 0.25 mm ID • Max. operating pressure: 200 bar • Operating temperature range: -51 °C to 50 °C
PEEK Tubing	• 1/8" OD x 1.6 mm ID • Max. operating pressure: 276 bar

3.7 Experimental Procedure

3.7.1 Solution Preparation

A 10 wt.% Illite clay slurry prepared in NaCl brine was used to coat the glass capillary tubes and the resealable glass micromodels. The concentration of clay was selected based on several trial experiments to avoid the clogging of the channels and have sufficient clay particles to be adsorbed on the surface. The primary reason for using NaCl brine as the base fluid is to represent the subsurface reservoir environment and prevent in situ fines migration and clay swelling caused by freshwater interaction with clay.

Slurries prepared with brines of four different salinities were used to evaluate the effect of salinity on clay adsorption to the glass surface. The brine properties are listed in table 3. As the solvent salinity was increased, the clay particles were more inclined to aggregating and settling down due to the decrease in the double layer repulsive forces. Therefore, to keep the particles dispersed in the solution, the clay slurries were stirred vigorously for 30 minutes, followed by ultrasonication using Branson 2800 Ultrasonic Cleaner for 1 hour and immediately injected into the capillary tubes.

3.7.2 Clay Coating Procedure

Glass capillary tubes were coated with Illite clay mainly to develop the coating procedure and study the effect of salinity on clay adsorption to the glass surface. Literature review revealed that there had been mainly two mechanisms of getting surface coated with geomaterials: physical adsorption [12, 20] and a layer by layer deposition of the minerals on the substrate surface [21, 56]. In the former method, the mineral slurry is flowed through the substrate surface, whereas in the latter case, a polyelectrolyte is used to link between the solid substrate and the coating minerals. Because in the latter case, the deposition is governed by electrostatic attractions among the substrate surface, polyelectrolyte, and minerals, the coating is more stable than that can be achieved from mere physical adsorption.

Despite this fact, in this study, the former method is used to develop the coated surface to achieve multiple objectives: avoid using any foreign synthetic compounds, replicate the subsurface porous environment as much as possible, and study the effect of salinity on physical adsorption to the glass surface. The process is adapted from Song et al. (2015) but modified to improve the coating density and stability [20].

Song et al. (2015) injected the clay slurry into the micromodel for several pore volumes, and prior to drying the surface, used airflow to displace the injected slurry [20]. However, we have noticed that the forward infusion of air causes the air to create a preferential flow path, and a large portion of clay slurry remains unswept by the air, affecting the uniformity of the coating. To improve the sweep efficiency, a faster flow rate or narrower flow network could be employed. However, either way, it will require a significantly faster flow rate that may wash away the adsorbed clay particles. Therefore, a more practical and universal solution was required.

In this study, instead of infusing air through the inlet to displace the clay slurry, the clay slurry was withdrawn by creating a vacuum at the outlet. This way, it was possible to avoid the air channeling without increasing the flow rate.

Since physical adsorption is driven by the Van der Waals attractive forces between the glass surface and clay particles, 100 cycles of clay solution infusion and withdrawal were performed to increase the contact of clay particles with the glass surface. Each cycle was composed of three steps: infusion-delay-withdrawal. Prior to injecting, the solid substrates were cleaned with Nitrogen Plasma using PE-50 Plasma Cleaner purchased from Plasma Etch, USA, to improve the hydrophilicity.

The clay solutions were required to be ultrasonicated every ten cycles to keep the particles dispersed in the solution. Fluids were infused into the capillary tubes at a velocity of 26.5 meters/hour using the syringe pump. Once the channel was completely saturated with clay slurry, fluids were

withdrawn at 2.65 meters/hour. A delay of 2 minutes between infusion and withdrawal was maintained to allow sufficient time for the clay particles to get adsorbed. The flow rates were selected based on several trial tests to deliver the clay slurry evenly into the flow volume and displace the fluid carrying unadsorbed and loosely attached particles without affecting the coating. A simplified schematic of the clay coating process for glass capillary tubes is shown in figure 16. Following the coating, the capillary tubes were air-dried at 25 °C for 1 hour. A very similar procedure was used to coat the resealable flow cells (Fig. 17). However, unlike the capillary tubes, the resealable flow cells had the facility to visualize the surface after each coating cycle, and only three cycles were observed to be sufficient to coat the glass surface uniformly; hence, the remaining cycles were not performed.

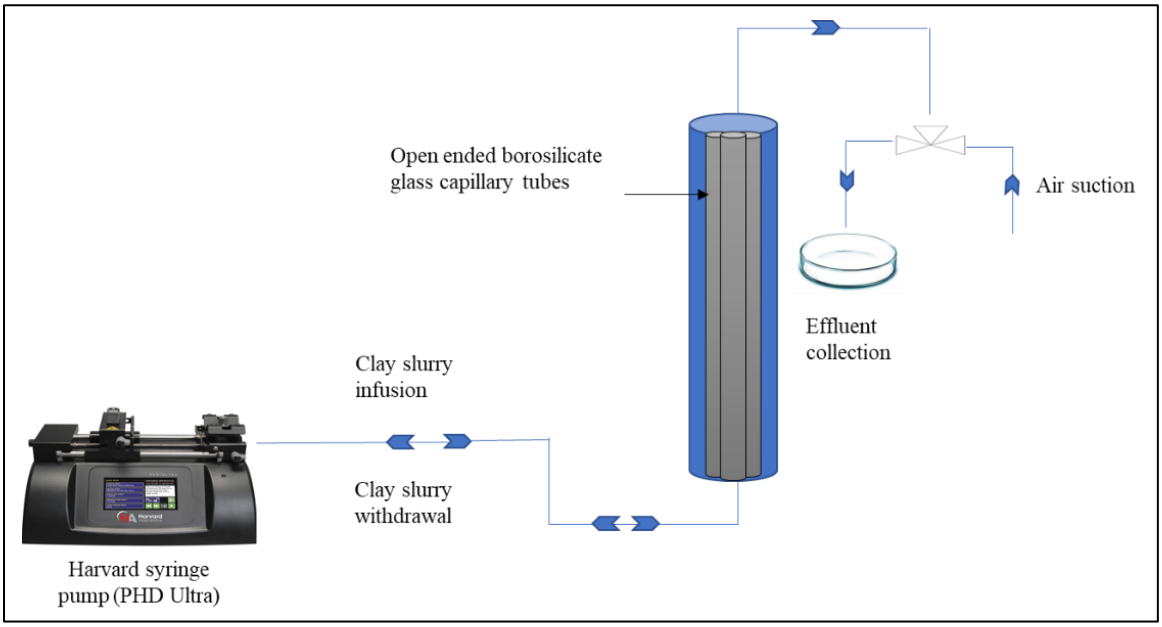

Figure 16: Schematic of coating glass capillary tubes with Illite clay

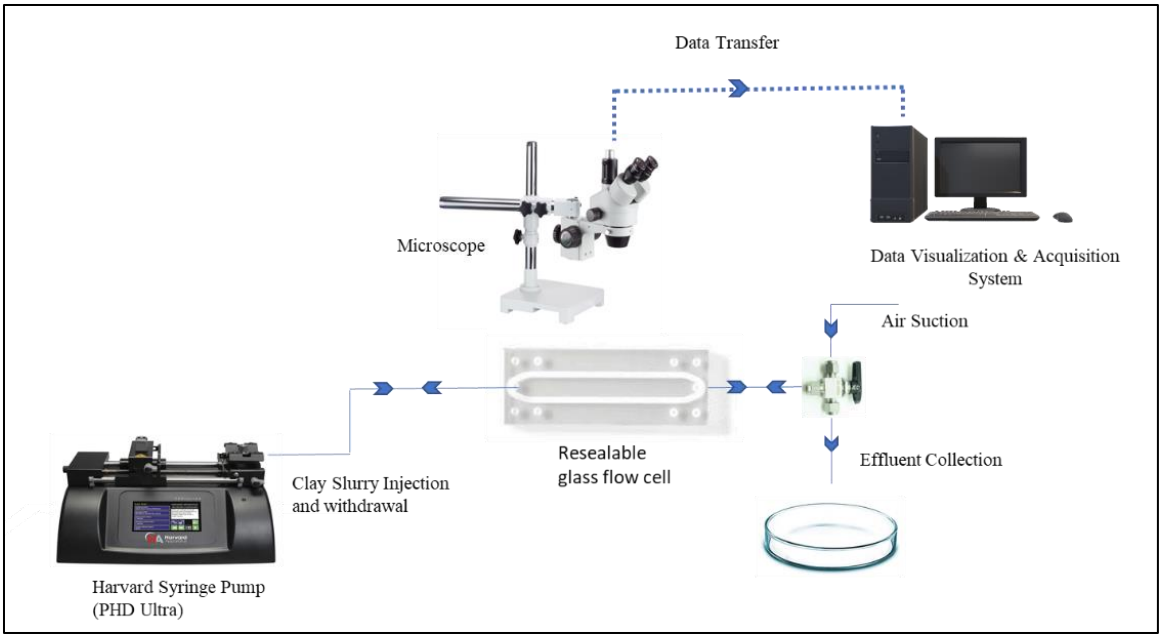

Figure 17: Schematic of coating resealable glass flow cell with Illite clay

3.7.3 Coating Characterization

After drying, the capillary tubes were carefully broken into small pieces by gently pressing them with a tweezer to expose the coated surfaces for microscopic characterization. Coating coverage and uniformity were evaluated by AmScope 10X LED optical microscope, morphology by FEI Quanta 600 field-emission gun Environmental Scanning Electron Microscope (SEM), and elemental atomic percentages by Bruker Energy-Dispersive X-ray Spectroscope (SEM-EDS).

3.7.4 Evaluating Effect of Salinity

To evaluate the effect of base fluids salinity on the adsorption of Illite particles to the glass surface, four different clay slurries were prepared: three with NaCl brines of three different salinities: 30,000 ppm, 10,000 ppm, and 5000 ppm and one with deionized water (DIW). The deionized water represented the base fluid with no salinity. The clay slurries were injected into the glass capillary tubes using the same infusion-delay-withdrawal protocol described in the previous section.

Following the coating, the surfaces were air-dried at 25°C for one hour and afterward characterized with the bright-field optical microscope, scanning electron microscope, and Energy-Dispersive X-ray Spectroscopy.

3.7.4.1 Approximating Coating Density

Each clay-coated surface was analyzed with Fiji, a distribution of ImageJ software bundled with pre-installed core ImageJ plugins to approximate the coating density.

In this study, the high magnification images (20X) of the glass surfaces coated with clay slurry prepared with different brines were converted to 8-bit grayscale images. Afterward, an ImageJ built-in global thresholding method, 'Moments' [57], was used to automatically set lower and upper threshold values to segment the grayscale image into features of interest (clay particles) and background (uncoated glass surface). Thresholding segments any grayscale image into 'foreground' and 'background' based on the pixel intensity. ImageJ software (Fiji) can then measure objects of the thresholded image according to the parameter set. It works by scanning and finding the edges of the objects. The detailed procedure can be found in ImageJ documentation of analyzing particles [58].

Before analyzing the particles, a region of interest (ROI) is selected that ignores any portion of the image that is out of focus. Then from the *Analyze* menu *Analyze Particle* command is used to measure the particle coverage over the selected region. It should be noted that the measurements made this way may vary due to the quality of the image and the thresholding algorithm selected [56]. Nonetheless, it serves the purpose of approximating coating density.

3.7.4.2 Zeta Potential Measurement

To understand the role of zeta potential on the adsorption of clay to the glass surface zeta potential of the clay solutions were measured with NanoBrook ZetaPALS purchased from Brookhaven

Instruments that uses the dynamic light scattering (DLS) method to determine the electrophoretic mobility of the colloid particles and calculate the surface zeta potential.

In this method, the solution needs to be water-clear so that light can scatter properly. Therefore, the 10 wt.% clay solutions could not be used as that high concentration would make the solution very cloudy and inappropriate for measurements. So instead, we used a range of clay concentrations from 0.05 wt.% to 1 wt.% to get the trend and extrapolate the result for higher concentration (10 wt.%).

3.7.5 Heat Treatment and Coating Stability Analysis

After the clay coating, the surface needs to be dried to make the particles adhered to it and achieve stability of the coating. For this purpose, the previous researchers have applied different techniques that include heat drying the coated surface in an oven or with a heat gun, air drying, hot air drying at different temperatures, and for different time intervals [12, 15, 20, 59].

In this study, the effect of heat treatment on the stability of the coating is evaluated. For this purpose, straight channel resealable glass micromodels were coated with 10 wt.% Illite clay slurry prepared in 30000 ppm NaCl solution. Two different post-coating treatments were used to dry the coated micromodels. The first treatment involved drying the surface with air at standard room temperature (25 °C) for 1 hour, while in the second method, the clay-coated surfaces were air-dried gradually up to 125 °C for 25 minutes, respectively.

To evaluate the sensitivity of the coated surface to the fluid flowing on it, the micromodels were exposed to flooding of base brine (30000 ppm) and the brines of reduced salinity (10,000 ppm and DI water) for six hours. The brines were prepared by dissolving NaCl powders in deionized water. After each flooding, vacuum suction was employed to take away loosely attached clay particles and brine. The fluid flow was conducted at the rates specified in Table 6. These flow rates were chosen to maintain a low capillary number (1×10^{-6}) so that the release of clay particles during the

flow is driven by clay-fluid interaction, not by viscous force. However, at the beginning of the injection, a faster flow rate (0.5 mL/min) was used for a volume of 400 µL to ensure that the brine completely saturates the flow cell. The coated surface was continuously monitored with an optical microscope to observe the coating's sensitivity to the brines and evaluate each treatment's effectiveness. Afterward, the surfaces were dried in the oven at 100 °C for 30 minutes to get away with any water left on the glass surface.

Table 7: Specifications of the brines used to study the stability of the coating after each heat treatment. Viscosities are calculated from empirical correlation [60]. Since the fluids are water-based, surface tensions are approximated to be equal to fresh water

Brine conc., ppm	Dynamic viscosity at 25°C cP	Surface tension, N/m	Capillary number	Flow rate, µL/min	Micromodel volume, µL	Pore volumes injected
30000	0.948	0.072	1×10^{-6}	32.19	300	37.73
10000	0.909	0.072	1×10^{-6}	33.58	300	39.39
5000	0.893	0.072	1×10^{-6}	34.18	300	40.11
0	0.892	0.072	1×10^{-6}	34.22	300	40.16

3.7.1.1 Microscopic Characterization of Coating Stability

Following oven-drying, the brine exposed resealable chips were disintegrated. Then, the bottom wall was evaluated with optical and SEM microscopy to observe the coating state after each flooding. It should be noted that the bottom wall of the flow cell had a slightly higher coating density than the top one, hence used for the microscopic analysis. This might be due to the effect of gravity that led to the increased deposition of clay particles on the bottom wall. This observation was consistent with the findings by Zhang et al. (2019) [49].

Confocal laser scanning microscopy was used to develop the 3D reconstructed images of the mineral coatings over the glass surface following each stability test. The surfaces were excited with 488 nm laser lines, and no fluorescent dyes were added to the samples as the clay particles were auto-fluorescent. Each of the surfaces was divided into a number of slices based on the focus planes,

and 2D images taken under the bright-field mode from each of the slices were stacked together to make 3-D reconstructed images of the optical section of the sample. The 3D images provided insights into the effectiveness of heat treatment on the stability of the coating.

CHAPTER IV

RESULTS AND DISCUSSION

4.1 Functionalizing Glass Capillary Tubes with Illite Clay

Figure 18 shows bright-field microscopic images of the uncoated glass capillary tube surface and the surface coated with 10 wt.% Illite clay slurry prepared in 30,000 ppm of NaCl solution. With this combination of the solution, a nearly uniform distribution of clay particles was observed on the glass surface, indicating the efficacy of the developed coating procedure.

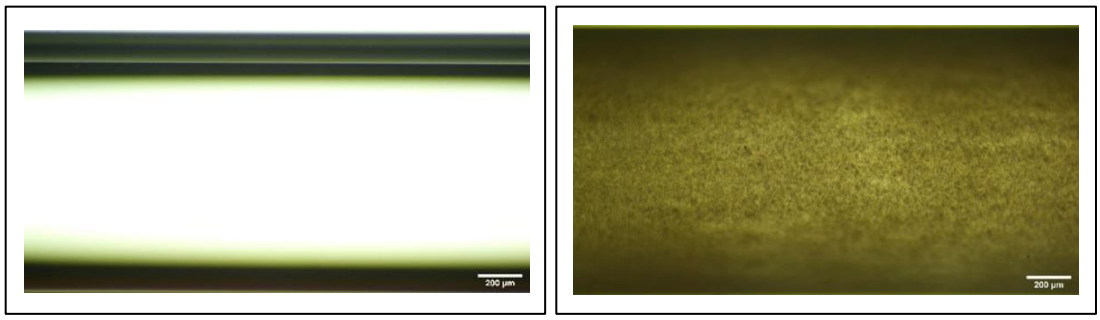

Figure 18: Microscopic image of the uncoated (left) and Illite-coated (right) glass capillary tube surfaces.

4.1.1 Microscopic Characterization of Coating

Figure 19 shows the Scanning Electron Microscopic (SEM) image of the coated surface at different magnifications. SEM-EDS elemental map of the coated surface is shown in figure 20. Oxygen, Silicon, Aluminum, Potassium, Iron, and Magnesium were the major chemical elements present

in the Illite clay (IMt-1) used to coat the glass capillary tubes (Table 2). EDS elemental map indicates the presence of those components on the coated surface as well. Even though a trace amount of Na is present in the clay, Na and Cl displayed in the elemental map were mainly associated with the brine used to prepare the clay slurry.

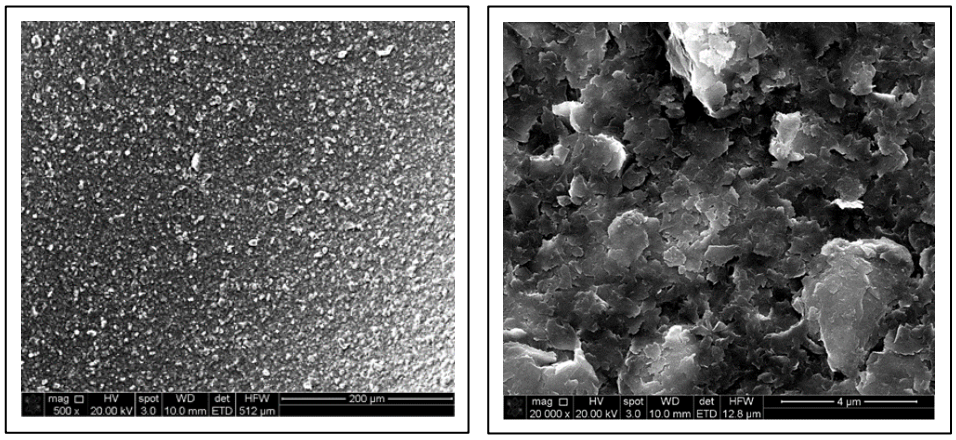

Figure 19: SEM image of the Illite-coated capillary tube surface at two different magnifications

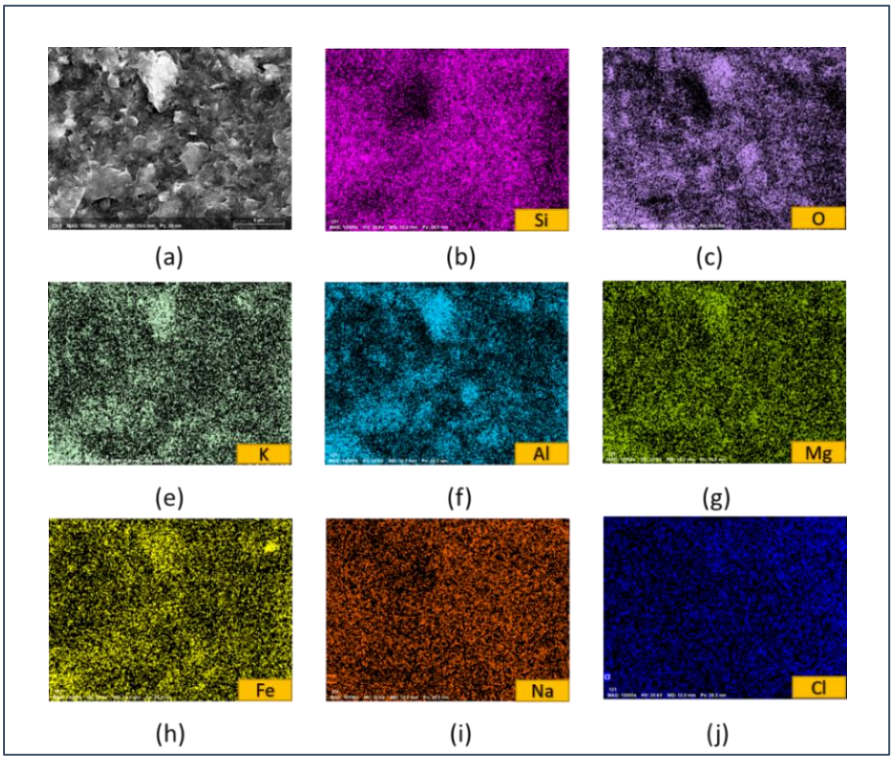

Figure 20: (a) SEM image and (b-j) EDS elemental map of the Illite coated glass capillary tube surface

4.1.2 Morphology of Coating

There were primarily two different kinds of objects visible on the higher magnification SEM images of the clay-coated surface (Fig. 21). EDS multi-object analysis was used to identify them. Object_1 and Object_2 are the bright spots in the foreground representing the group of grainier particles, and Object_3 and Object_4 are the black spots representing the finer ones. The wt.% range of the elements in the composite mass for each object displayed in table 8 and figure 22 reveals that each object has an almost similar chemical composition. The slight difference in the mass composition could be due to the differences in the size of clay particles and variation in the coating thickness.

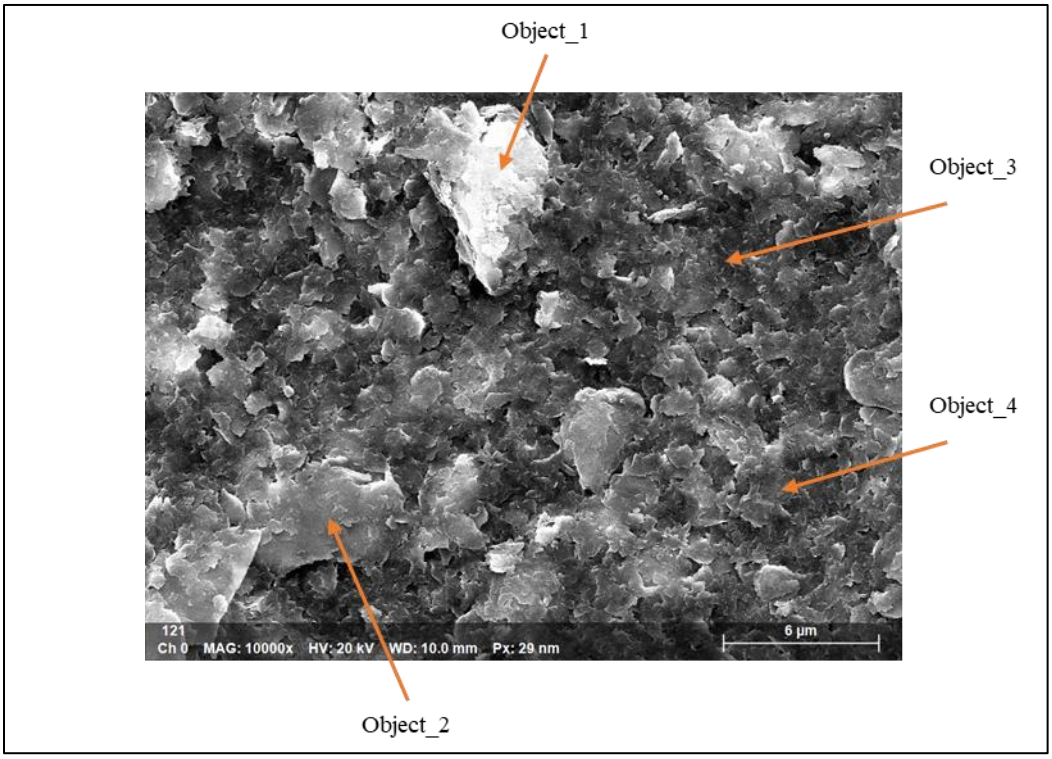

Figure 21: SEM image of the clay-coated capillary tube surface showing different sizes of objects

Table 8: Elemental wt.% associated with each object obtained from SEM-EDS multi-object analysis of the Illite-coated capillary tube surface

Spectrum	C	O	Na	Mg	Al	Si	Cl	K	Ca	Fe
obj_1	6.6	47.8	1.0	1.4	11.9	21.8	0.3	5.7	0.1	3.5
obj_2	6.5	41.5	0.6	1.1	10.8	29.2	0.1	5.7	0.0	4.4
obj_3	6.4	41.4	0.9	0.6	7.0	37.7	0.3	3.5	0.1	2.1
obj_4	6.8	41.2	1.1	0.8	8.2	34.2	0.2	4.2	0.1	3.1
Mean	6.6	43.0	0.9	1.0	9.5	30.7	0.2	4.8	0.0	3.3

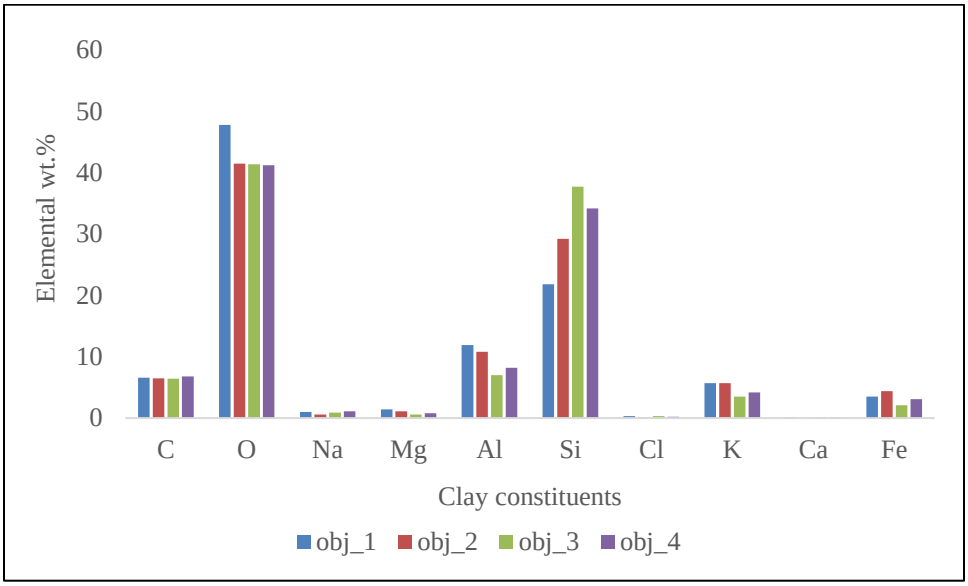

Figure 22: Chart showing the elemental composition of each of the objects. The similarity in the objects' elemental composition indicates the presence of nothing but clay particles on the coated surface. Slight variation in the wt. % might be due to the variation in the size of clay particles and the coating thickness

4.2 Effect of Salinity on Clay Coating

Glass capillary tubes coated with 10 wt.% Illite clay prepared in NaCl solutions of four different concentrations (0 ppm, 5000 ppm, 10000 ppm, and 30000 ppm) were created. Figure 23 shows the optical microscopic images of the surfaces coated with those different clay slurries. It is observed that as the brine concentration is increased, the coating coverage is improved. When the clay slurry was created with DI water, there was seemingly no adsorption of the clay particles on the glass

surface. However, with higher concentrations of brine, the number of adsorbed particles increased, and with 30000 ppm, a quasi-homogeneous coating was observed.

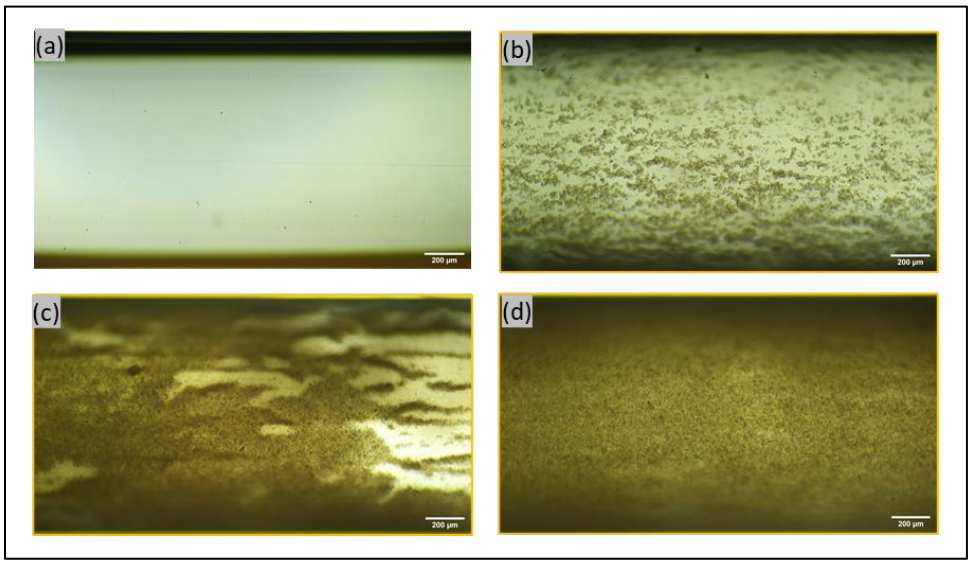

Figure 23: Glass capillary tubes coated with 10 wt.% Illite clay slurry prepared with Illite: (a) DI water, (b) 5000 ppm NaCl, (c) 10000 ppm NaCl, and (d) 30000 ppm NaCl. Images are taken after drying the coated capillary tubes at 25 °C. Clay solution prepared with higher salinity of brine produced better coating in terms of coverage and uniformity

EDS elemental map of the coated surface has also exhibited increased adsorption of clay particles on the glass surface when the slurry is prepared with the high salinity brine (Fig. 24). Figure 24 (a) shows that the surface coated with clay slurry prepared in 5000 ppm of brine has the elemental map dominated by the presence of silicon (Si). Even though Si is the primary constituent of both the solid substrate and the clay minerals, the significant dominance of silica here indicates the uncoated borosilicate glass surface as the primary source of it. Otherwise, there would also have a significant contribution of other clay components (e.g., Mg, Al, K, Ca, Fe, etc.) on the elemental map similar to figure 24 (b) and figure 24 (c). Increased concentration of brine (10,000 ppm and 30,000 ppm) there resulted in increased adsorption of clay particles. As a result, the coated surfaces display more distribution of other clay constituents besides Si on the EDS elemental map (Fig. 24 (b) and 24 (c)),

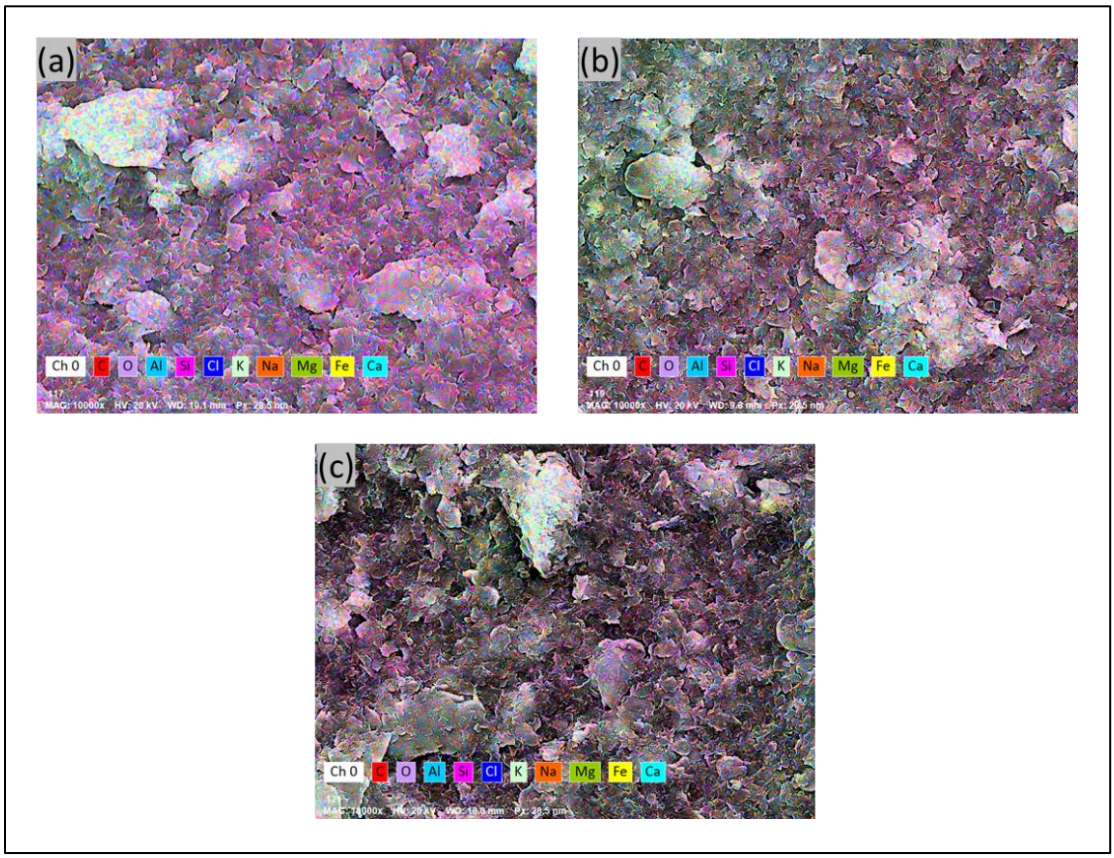

Figure 24: EDS elemental distribution maps of glass surfaces coated with Illite clay prepared in (a) 5000 ppm, (b) 10000 ppm, and (c) 30000 ppm of NaCl solution. The color indexes are showing the presence of different chemical elements on the coated surface. For example, figure 24 (a) being dominated by purple color indicates less amount of clay adsorption on the glass surface, rendering the surface mostly uncoated. With the increased salinity of brine, a more balanced distribution of clay constituents is displayed in figure 24 (b) and figure 24 (c)

4.2.1 Approximating Coating Density

The coating density was approximated by image analysis of the micrographs using Fiji software. The high magnification (20X) optical image of the Illite-coated capillary tube surfaces and the 8-bit grayscale and the thresholded image generated from it is shown in figure 25. The surface attempted to coat with clay-deionized water is not included in the coating density approximation as there was hardly any adsorption of clay particles to the glass surface when the clay slurry was prepared with DIW, as seen in figure 23.

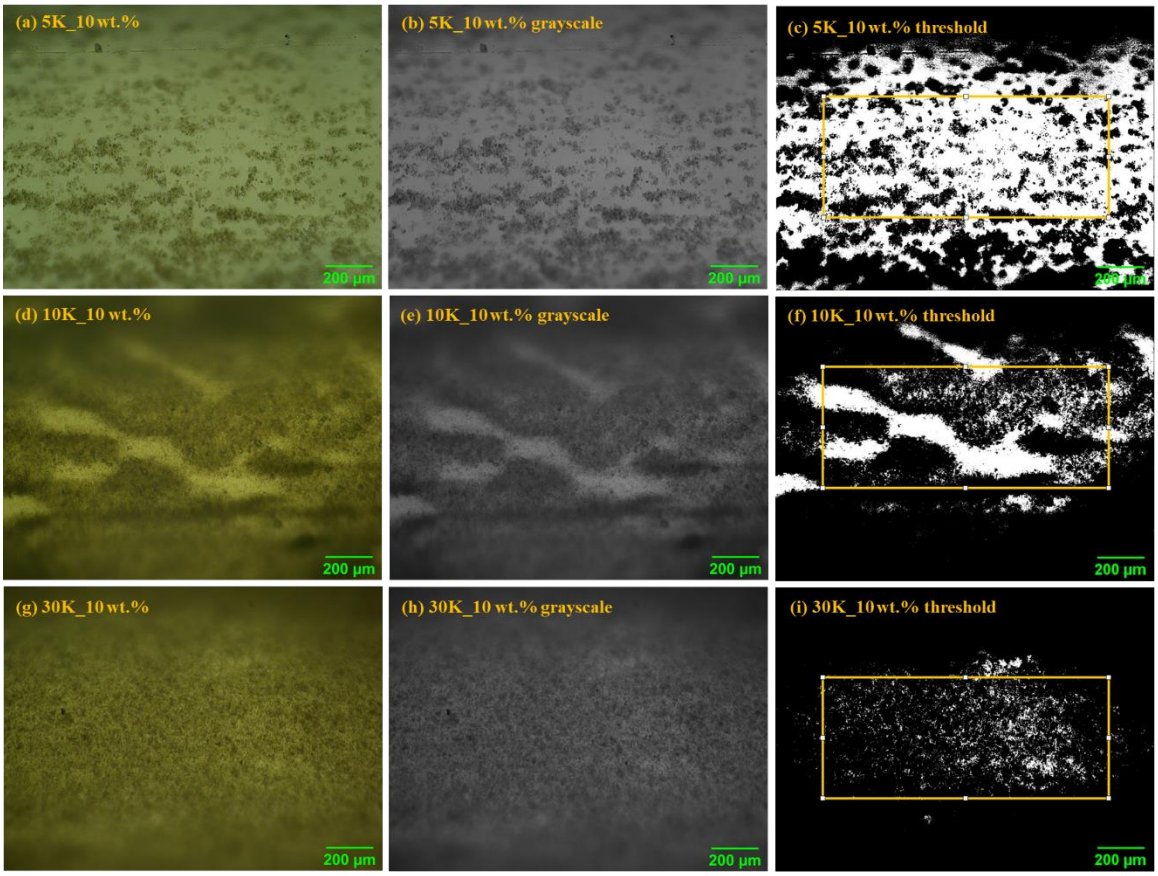

Figure 25: High magnification (a, d, g) optical, (b, g, h) 8-bit grayscale, and (c, f, i) threshold images of the capillary tube surfaces after coating with clay slurry prepared in (a-c) 5000 ppm, (d-f) 10,000 ppm, and (g-i) 30,000 ppm NaCl brine. The rectangular region is showing the ROI where the coating density is approximated

The coating coverage was around 20.5 % in the rectangular region of the surface coated with clay in 5000 ppm of brine. When the surface was coated with clay in 10,000 NaCl brine, the coating coverage increased to ~ 45 %. Finally, with 30,000 ppm NaCl, almost 80% coating coverage was obtained. This higher coating density with high salinity brine (30,000 ppm NaCl) could be explained with the DLVO theory and attributed to the decreased electric double layer repulsive (EDL) forces between the clay particles.

It is well known that clay particles have a net negative charge on their surface. When the clay solution was prepared with deionized water, the effect of repulsive forces between the similarly

charged clay particles was too high for the Van der Waals attractive forces to adhere the clay particles on the glass surface. As the brine concentration increases, the number of counter-ions in the clay solution also increases. Those counter-ions were responsible for counterbalancing the negative surface charges of the clay particles. Hence, the EDL forces between the particles were diminished, and Van der Waals attractive forces between the particles and the glass surface became the dominant force driving the adsorption of clay particles to the glass surface.

4.2.2 Zeta Potential Characterization

Zeta Potential (ζ), often considered the effective charge of any colloid particles, provides insights into the forces acting between the particles. Since the value of ζ is proportional to the square root of the EDL force, charged particles (e.g., clay minerals) with a higher magnitude of ζ tend to have higher repulsive forces between them [61]. Therefore, to validate the effect of EDL on the observed adsorption of clay particles to the surface, the ζ values of the clay particles dispersed in the brine solutions were measured. However, possibly due to the rapid flocculation and sedimentation of the clay particles affecting the electrophoretic mobility of the particles, the ζ values had very high standard deviations between each run (Table 9). Therefore, the measurements were unreliable with the Light Scattering Method and needed to be suspended.

Table 9: Zeta Potential values measured with the Dynamic Light Scattering method. Measurement had to be abandoned due to the high standard deviation between each run. The measurement with deionized water was conducted with fewer runs to reduce the effect of clay settlement. Regardless, the standard deviation was too high to make the values reliable

Clay Concentration	Base Fluid	Mean ZP	No. of Runs	Std. Deviation
0.005	30000 ppm NaCl	-10.55	5	22.46
0.01	30000 ppm NaCl	-11.07	5	19.10
0.05	30000 ppm NaCl	-21.05	5	14.28
0.1	30000 ppm NaCl	-12.42	5	13.30
0.05	DIW	-3.86	3	7.81

4.3 Preparing Clay-Coated Micromodel

Figures 26 (a) and 26 (b) show the optical microscopic images of the uncoated resealable microfluidic chip (borosilicate glass) surface before injecting any fluid into the resealable microfluidic chip. Figures 26 (c) and 26 (d) are showing those surfaces covered with clay slurry after one cycle of injection. As can be deduced from the figures, the microfluidic chip was completely saturated with clay slurry.

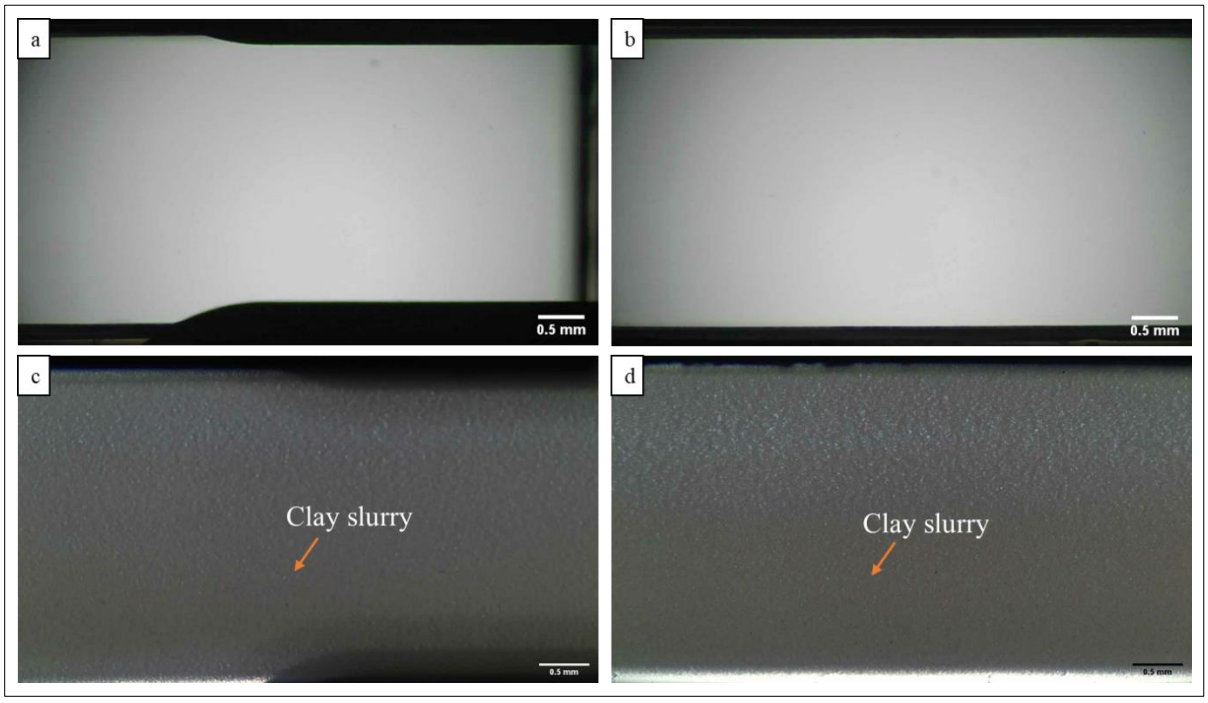

Figure 26: Optical microscopic images of the resealable microfluidic chip surface (a,b) uncoated, and (c, d) completely saturated with clay slurry at two different locations

Air was injected into the microfluidic chip to displace the clay slurry and have only the adsorbed particles on the surface. Figure 27 shows the narrow channeling of air through the clay-saturated microfluidic chip, which left a significant amount of clay slurry stagnant and unswept from the micromodel.

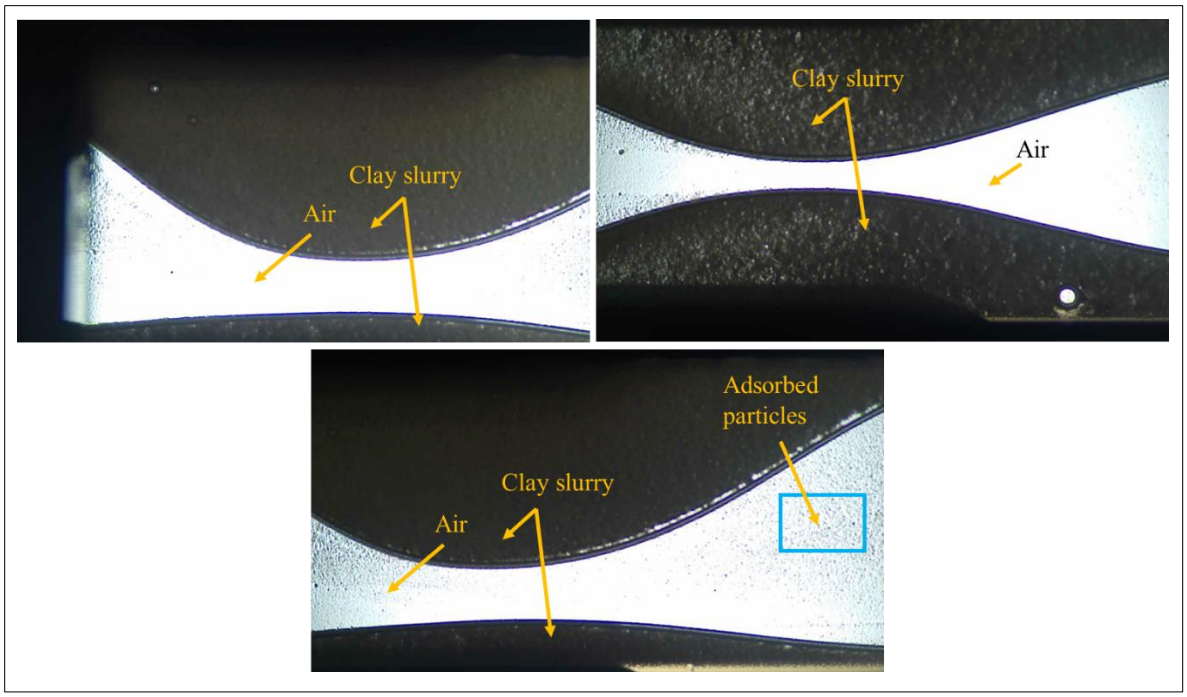

Figure 27: Air channeling and uneven deposition of clay particles resulting from the forward infusion of air to displace clay slurry

To solve this potential issue of air channeling, instead of infusing air through the inlet to displace the clay slurry, the slurry was withdrawn by creating a vacuum at the outlet with the syringe pump. The vacuum suction of air from the chip outlet resulted in a very effective displacement of clay slurry and uniform distribution of adsorbed particles on the glass surface (Figures 28 and 29).

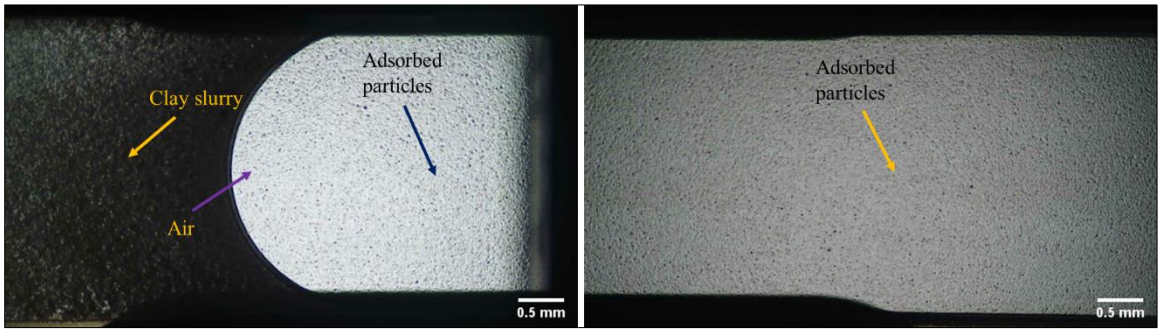

Figure 28: Vacuum suction leading to a (left) uniform displacement of clay slurry and (right) an even distribution of adsorbed clay particles on the glass surface after the complete withdrawn of the clay slurry

Figure 29: High magnification image of the dried micromodel surface after Illite-clay coating

4.3.1 Heat Treatment and Stability Analysis

The release of clay particles from the clay-coated surface could be due to the instability of the coating or the sensitivity of the clay particles to the fluid flowing on it. While the former one depends on how firmly clay particles are attached to the substrate surface or, in other words, the stability of the coating, the latter one is a function of salinity or the number of counter-ions present in the fluid. Brines with salinity less than the formation water (the high salinity water the clay surface was initially exposed to) cause detachment of the clay particles from the rock surface and are considered one of the primary mechanisms of wettability alteration in clay-rich formation due to low salinity water flooding [62, 63].

Prior to evaluating the stability of the coating, it is, therefore, crucial to distinguish the release of clay particles owing to the clay-brine interaction from that due to the instability of the coating. Since the clay particles were already in contact with 30,000 ppm NaCl brine as the clay slurry was prepared with it, 30,000 ppm NaCl brine could be considered, in this case, as the formation water. Thus, the coating can be considered stable if flooding of 30,000 ppm of NaCl brine for a sufficient

period of time does not cause a significant release of clay particles from the glass surface. Any fluid having salinity less than this should cause the release of clay particles, and the effect is expected to increase as the salinity of the injection fluid gets decreased. Having said that, none of the fluids should completely wash away the coating if the coating is really stable. It should also be noted that, for a successful preparation of the geomaterial model, the heat treatment should not make the clay particles completely immobile. Having a stable coating without compromising the natural mobility of the clay particles will make the geomaterial surface a close representative of the clay-rich rock surface.

4.3.1.1 Cay-coating Stability Characterization from Optical Microscopy

Figure 30 shows the optical microscopic images of the (a) initial state of the Illite-coated micromodel surface before flooding any fluid, state of the coated surface dried at (b) 25 °C and (c) 125 °C after exposed to 30,000 (30K) ppm NaCl brine, surface dried at (d) 25 °C and (e) 125 °C exposed to 10,000 (10K) ppm NaCl, and surface dried at (f) 25 °C and (g) 125 °C exposed to deionized water (DIW) for 6 hours during the dynamic flooding test. The locations from where the release of clay particles was visually identifiable are marked with red rectangles. Comparison between figure 30 (a), 30 (b), and 30 (c) indicate that the surface dried at 125 °C has more similarity in coating appearance with the initial state than the one dried at 25 °C, where the release of clay particles is visually detectable. This implies that drying the clay-coated micromodel at 125 °C temperature improves the stability of the coating.

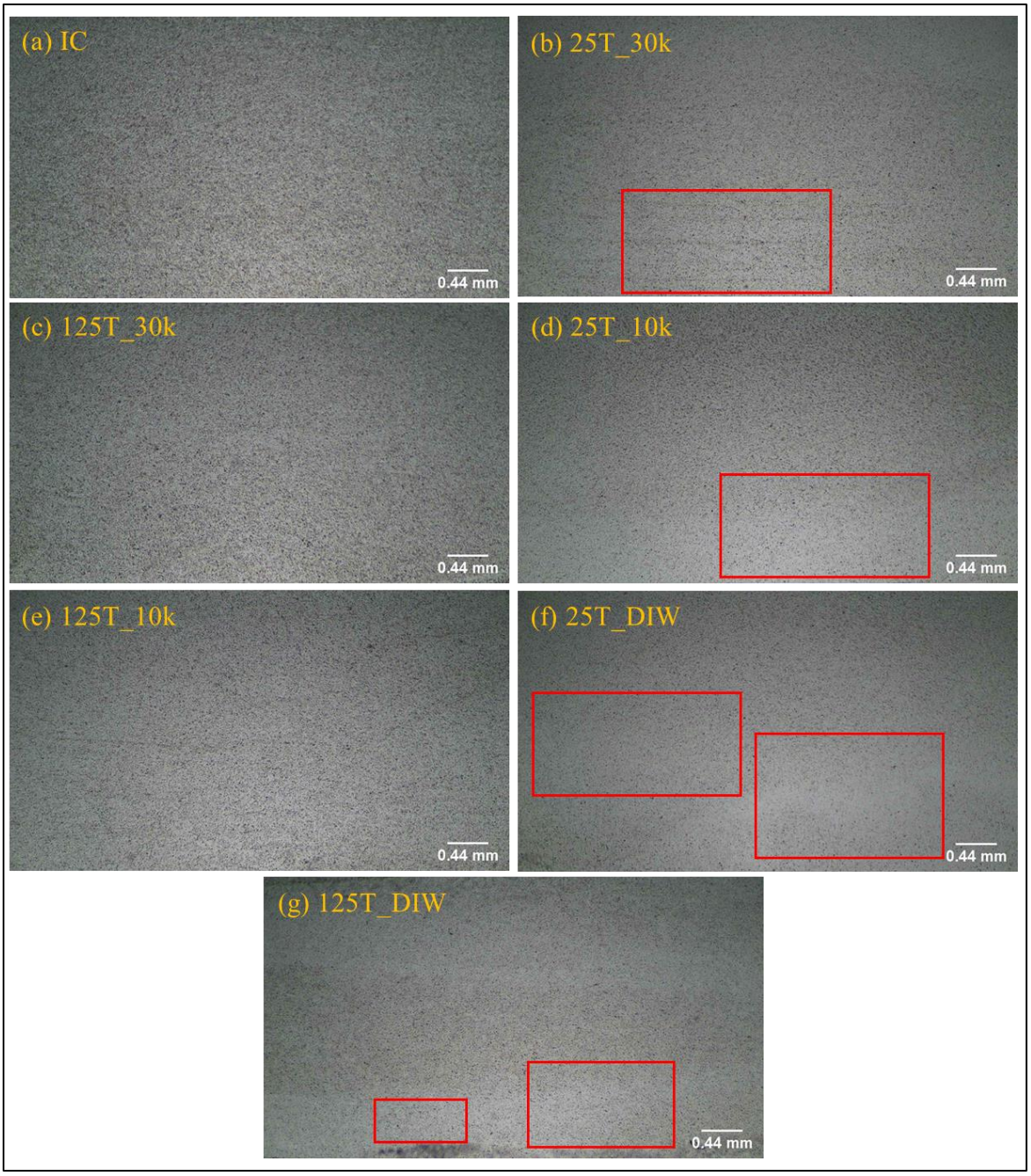

Figure 30: Optical microscopic images of the Illite-coated surfaces after exposed to brines of different concentrations and deionized water (DIW) for 6 hours. IC represents the initial condition of the coated surface before flooding and without the heat treatment. 30K and 10K represent the 30,000 ppm and 10,000 ppm NaCl brine used to wet the coated surface, respectively. Red rectangles are showing some of the washout zones in the coated surface from where the clay particles are washed away or might have migrated to other locations as the surface came in contact with the liquids

Figures 30 (d-g) reveal that, regardless of what temperature was used to dry the coated surface, fluids with salinity less than 30,000 ppm of brine caused detachment of the clay particles in both types of surface. This implies that the heat treatment did not make the coating completely immobile. However, the degree of sensitivity of the clay particles with the brines was affected by the heat treatment. Compared to the Illite-coated surfaces dried at 25 °C, the surfaces treated at 125 °C temperature retained more particles attached to the surface following the flow of less salinity brines and deionized water.

4.3.1.2 Stability Characterization using Scanning Electron Microscopy

Figure 31 shows the scanning electron microscopic (SEM) images of the coated micromodel surfaces after the dynamic flooding test. For the SEM images, lower magnification images are displayed to obtain a wider field of view. Similar to optical images, SEM images also exhibit a resemblance in the coating appearance between the initial condition (Figure 31 (a)) and the 125 °C treated surface exposed to 30,000 ppm brine flooding (Figure 31 (e)). However, unlike the optical image (Figure 30 (b)), SEM image of the 25 °C treated surface (Figure 31 (b)) shows a relatively denser coating than the initial state (Figure 31 (a)). This might be due to the very small field of view usually associated with SEM images and localized accumulation of clay particles being migrated from another location of the surface. Nevertheless, this also implies that the 25 °C treated surface was more prone to clay detachment than the one treated at 125 °C.

The effect of heat treatment is more evident in the SEM images of the coated surfaces exposed to low salinity brines (salinity < 30,000 ppm) and deionized water (Fig. 31 (c), 31 (d), 31 (f), and 31 (g)). Even though the release of particles is visible in both types of surfaces, the surface-treated at 25 °C was affected the most.

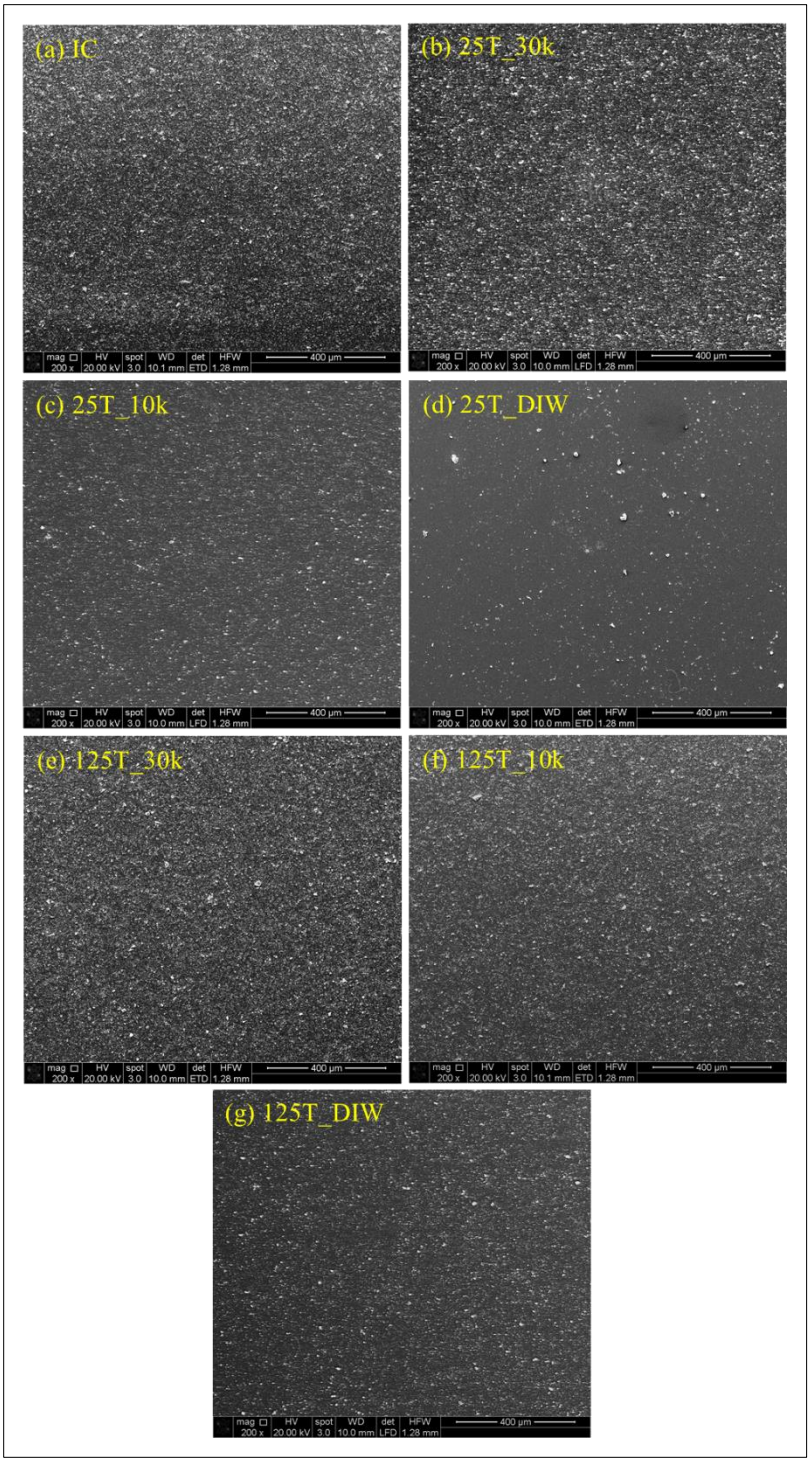

Figure 31: SEM images of the coated surfaces after exposed to brines of different concentrations for 6 hours. Figure 31 (a) shows the initial state of the coated surface before flooding any fluid; (b) state of the coated surface dried at 25 °C after exposed to NaCl brines of 30,000 ppm (30K), (c) 10,000 ppm (10K), and (d) deionized water (DIW) for 6 hours; Figure 30 (e) shows the state of the coated surface dried at 125 °C after exposed to NaCl brines of 30K ppm, (f) 10K ppm, and (g) DIW for 6 hours.

4.3.1.3 Stability Characterization using Confocal Laser Scanning Microscopy

Confocal laser scanning microscopy (CLSM) was used to further confirm the improved stability of the coated surface treated at 125 °C. Figure 32 shows the 3D reconstructed images of the coated surfaces after being exposed to 30,000 ppm of NaCl brine and deionized water. The surfaces were excited with 488 nm laser lines. No fluorescent dyes were applied to the auto-fluorescent clay minerals. Clay particles adsorbed the laser lights and caused the green fluorescence visible in figure 32.

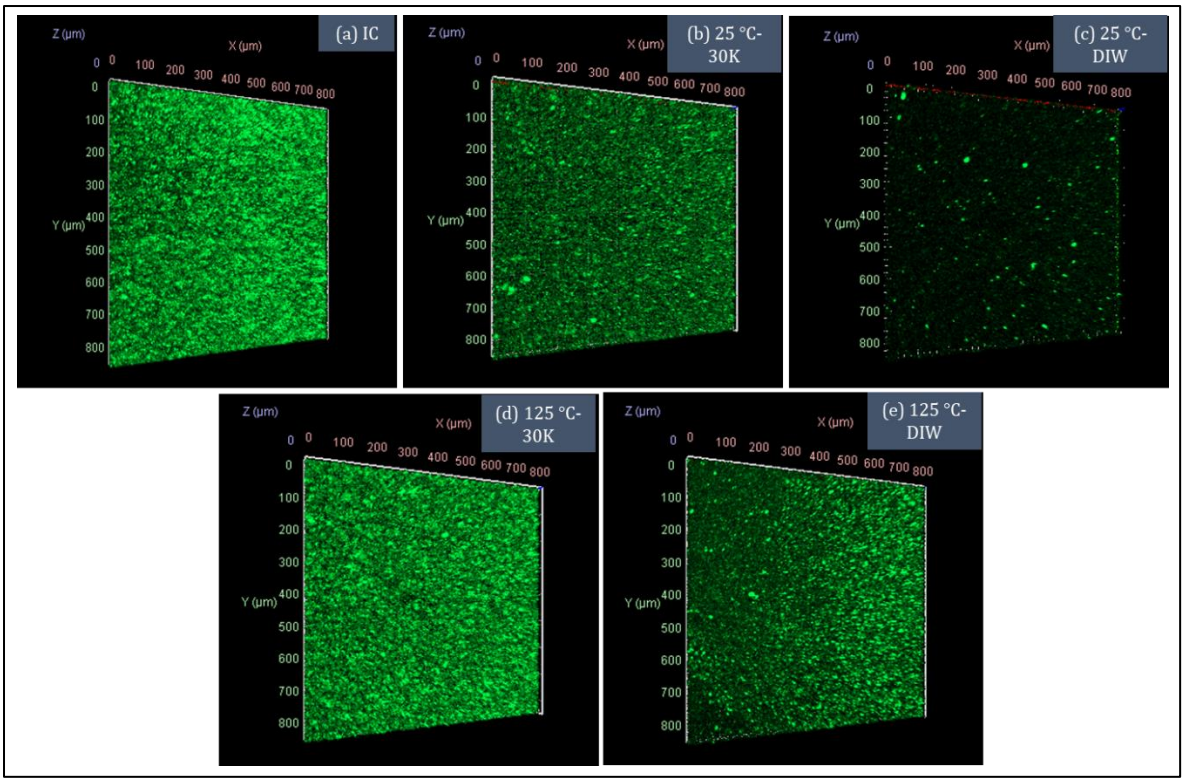

Figure 32: 3D reconstructed images of the mineral coatings over the glass surface showing the state of coating at different conditions:(a) The initial condition of the coated surface before flooding any fluid ; (b-c) state of the coated surface dried at 25 °C after being exposed to 30,000 ppm (30K) of NaCl brine and deionized water (DIW) for 6 hours; (d-e) state of the coated surface dried at 125 °C after being exposed to 30,000 ppm of NaCl brine and deionized water for 6 hours. Each image has the size of 848.53 µm × 848.53 µm × 40.5 µm.

Following the 30,000 ppm brine flooding, the surface treated at 125 °C exhibited more similarity in coating appearance with the initial state of the coating than the one treated at 25 °C. The surface

dried at 25 °C and exposed to 30,000 ppm NaCl flow, displayed fewer green fluorescence when excited with the laser beams, indicates that a good number of clay particles have already been washed away from the surface.

The effect of heat treatment is more evident in the case of DI water flooding. Coating treated at 25 °C experienced a wash away of most of the clay particles during the DI water flooding, as it can be deduced from the dearth of green fluorescence in Figure 32 (e). However, even though 125 °C treated surface also experienced some release of clay particles due to DI water flow, thus corroborating the fact that natural mobility of the clay particles was not compromised by the heat-treatment, the 125 °C treated surface had considerably more clay particles remained attached to the surface following the flooding than the one treated at 25 °C. These observations are consistent with the findings from optical and SEM images.

CHAPTER V

CONCLUSION

This study aimed to generate an Illite-coated geomaterial micromodel that can represent the clay chemistry of Illite-rich shale formations such as Caney of Southern Oklahoma, USA. While doing so, the effect of base fluid's concentration on the adsorption of clay particles to the glass surface was evaluated. Dynamic flooding tests were also carried out to find out the effect of heat treatment on the stability of the coating. By analyzing the clay-coated surfaces with optical, SEM, and confocal microscopy, this thesis has shown how the concentration of base fluid and drying temperature can directly affect the quality of clay-coating.

In this study, Illite-coated surfaces were successfully generated in borosilicate glass capillary tubes and resealable straight channel microfluidic chips made of borosilicate glass. It was observed that forward infusion of air- a widely used approach of displacing clay solution from the channel- might cause narrow channeling of air inside the flow network and leave a large volume of clay slurry unswept. This may result in a very non-uniform and uneven deposition of clay particles on the glass surface when dried. This study provided a new approach to solve this issue that will not require increasing the flow rates. Instead of forward infusion, vacuum suction of air was used from the outlet of the chip to displace the clay slurry. This way, no-air channeling was observed inside the chip, and a very uniform and even distribution of clay particles were attained.

NaCl solution was used as the base fluid to prepare the clay slurry required to inject into the capillary tubes and microfluidic chip. The salinity of the NaCl solution was found to have a significant effect on the adsorption of clay particles to the glass surface. Based on the microscopic characterization and coating density approximation with Fiji, this study has shown that if the salinity or ionic concentration of the base fluid is increased, a more dense and uniform clay coating could be obtained on the glass surface. In this study, the slurry prepared with deionized water rendered no adsorption of clay particles on the surface, whereas with 30,000 ppm NaCl brine, a more uniform and dense distribution of clay particles was observed.

The study also reported a significant improvement of the coating stability once the clay-coated micromodels were dried at an elevated temperature (125 °C) for 25 minutes. The micromodel dried at the lower temperature (25 °C) performed poorly even when contacted with the high salinity brine (30,000 ppm NaCl). There were considerable detachments of the clay particles from the glass surface at different locations. Deionized water caused the maximum damage as several wash-away zones of the coated layer was visible in the optical, SEM, and CLSM images. In contrast, there were not such detachments of the clay particles from the glass surface when the 125 °C treated glass surface was exposed to the high salinity brine flooding for 6 hours. The temperature was enough to keep the particles firmly attached to the surface without compromising the natural mobility of the clay particles. The particles from few locations got eventually detached when the surface came in contact with less salinity brine and deionized water.

There were some obstacles faced during this research, primarily due to the instability of the clay solution. The study could not characterize the zeta potential of the clay slurries with the dynamic light scattering method that could help understand the underlying mechanism of clay particles not getting adsorbed in the glass surface when mixed with low salinity brine or deionized water. Future

studies can employ more advanced methods of measuring the zeta potential of the clay solution, such as liquid AFM that will not be affected by the instability of clay solutions.

There are other scopes as well for far more research with clay-coated microfluidics chips. The geomaterial micromodel developed in this study is a straight channel one having a single aspect ratio. Future studies could include developing a uniform coating on a more complex flow network with a very small channel width and different aspect ratios similar to the unconventional rocks. This way, the geomaterial micromodel would provide a more realistic representation of the clay-rich rock formations.

Nevertheless, while the larger width and single aspect ratio of the clay-coated micromodel developed in this study limit its ability to represent the capillary forces and ultra-low permeability of actual shale samples, the developed Illite-coated surface can mimic the physicochemical aspects of the shale formations, especially the clay-chemistry. Given the significance of clay-fluid interaction on the exploitation of hydrocarbons from clay-rich shale formations, the clay-coated model developed from this study, therefore, will be very useful to study the behavior of clayey formations (e.g., swelling potential, fines migration, wettability alteration, etc.) upon exposure to drilling, fracking or any other injection fluids. However, to do so, further research is needed to develop the methods of quantifying clay behaviors such as swelling potential and fines migration in microfluidics. The information can then be used to design injection fluids to avoid clay-induced problems and optimize hydrocarbon production from shale formations.

REFERENCES

1. Shaw, D.B. and C.E. Weaver, *The mineralogical composition of shales.* Journal of Sedimentary Research, 1965. **35**(1): p. 213-222.
2. Rahman, M., et al., *Unsuccessful hydraulic fracturing cases in Australia: Investigation into causes of failures and their remedies.* Journal of Petroleum Science and Engineering, 2007. **57**(1-2): p. 70-81.
3. Zhou, Z., et al., *Effect of clay swelling on reservoir quality.* Journal of Canadian Petroleum Technology, 1996. **35**(07).
4. Rogala, A., et al., *Non-aqueous fracturing technologies for shale gas recovery.* Physicochemical Problems of Mineral Processing, 2013. **49**.
5. Song, W. and A.R. Kovscek, *Direct visualization of pore-scale fines migration and formation damage during low-salinity waterflooding.* Journal of Natural Gas Science and Engineering, 2016. **34**: p. 1276-1283.
6. Stephens, M., S. Gomez-Nava, and M. Churan. *Laboratory methods to assess shale reactivity with drilling fluids*. in *AADE National Technical Conference, New Orleans*. 2009.
7. Gomez, S.L. and W. He. *Fighting wellbore instability: customizing drilling fluids based on laboratory studies of shale-fluid interactions*. in *IADC/SPE Asia Pacific Drilling Technology Conference and Exhibition*. 2012. Society of Petroleum Engineers.
8. Sayegh, S., et al., *Rock/fluid interactions of carbonated brines in a sandstone reservoir: Pembina Cardium, Alberta, Canada.* SPE Formation Evaluation, 1990. **5**(04): p. 399-405.
9. Somerton, W. and C. Radke, *Role of clays in the enhanced recovery of petroleum from some California sands.* Journal of Petroleum Technology, 1983. **35**(03): p. 643-654.
10. Amirian, T., *Pore-scale visualisation and geochemical modelling of low salinity water flooding as an enhanced oil recovery method*. 2019, University of Adelaide.
11. Amirian, T. and M. Haghighi, *Impact of clay type and water composition on low salinity water injection–visualisation approach.* The APPEA Journal, 2018. **58**(1): p. 51-59.
12. Amirian, T., M. Haghighi, and P. Mostaghimi, *Pore scale visualization of low salinity water flooding as an enhanced oil recovery method.* Energy & Fuels, 2017. **31**(12): p. 13133-13143.
13. Anbari, A., et al., *Microfluidic model porous media: fabrication and applications.* Small, 2018. **14**(18): p. 1703575.

14. Berg, S., et al., *Direct experimental evidence of wettability modification by low salinity.* Petrophysics - The SPWLA Journal of Formation Evaluation and Reservoir Description, 2010. **51**(05).
15. Bondino, I., et al. *Visual microscopic investigations about the role of pH, salinity and clay on oil adhesion and recovery*. in *International Symposium of the Society of Core Analysts held in Napa Valley, California*. 2013.
16. Bowden, S.A., et al., *Recreating mineralogical petrographic heterogeneity within microfluidic chips: assembly, examples, and applications.* Lab on a Chip, 2016. **16**(24): p. 4677-4681.
17. Gerami, A., et al., *A microfluidic framework for studying relative permeability in coal.* International Journal of Coal Geology, 2016. **159**: p. 183-193.
18. Gunda, N.S.K., et al., *Reservoir-on-a-Chip (ROC): A new paradigm in reservoir engineering.* Lab on a Chip, 2011. **11**(22): p. 3785-3792.
19. Oh, Y.S., et al., *A microfluidic approach to water-rock interactions using thin rock sections: Pb and U sorption onto thin shale and granite sections.* Journal of Hazardous Materials, 2017. **324**: p. 373-381.
20. Song, W. and A.R. Kovscek, *Functionalization of micromodels with Kaolinite for investigation of low salinity oil-recovery processes.* Lab on a Chip, 2015. **15**(16): p. 3314-3325.
21. Zhang, Y., A. Sanati-Nezhad, and S. Hejazi, *Geo-material surface modification of microchips using layer-by-layer (LbL) assembly for subsurface energy and environmental applications.* Lab on a Chip, 2018. **18**(2): p. 285-295.
22. Barnaji, M.J., P. Pourafshary, and M.R. Rasaie, *Visual investigation of the effects of clay minerals on enhancement of oil recovery by low salinity water flooding.* Fuel, 2016. **184**: p. 826-835.
23. Mahani, H., et al., *Kinetics of low-salinity-flooding effect.* SPE Journal, 2015. **20**(01): p. 8-20.
24. Schembre, J., G.-Q. Tang, and A. Kovscek, *Wettability alteration and oil recovery by water imbibition at elevated temperatures.* Journal of Petroleum Science and Engineering, 2006. **52**(1-4): p. 131-148.
25. Guggenheim, S. and R. Martin, *Definition of clay and clay mineral: joint report of the AIPEA nomenclature and CMS nomenclature committees.* Clays and Clay Minerals, 1995. **43**(2): p. 255-256.
26. Marchuk, S., *The dynamics of potassium in some australian soils*. 2016.
27. Shainberg, I. and G.J. Levy, *Flocculation and dispersion,* in *Encyclopedia of Soils in the Environment*, D. Hillel, Editor. 2005, Elsevier: Oxford. p. 27-34.
28. MacEwan, D. and A. Ruiz-Amil, *Interstratified clay minerals,* in *Soil Components*. 1975, Springer. p. 265-334.
29. Poppe, L., et al., *A laboratory manual for X-ray powder diffraction.* US Geological Survey Open-File Report, 2001. **1**(041): p. 1-88.
30. Sawhney, B.L., *Interstratification in layer silicates.* Minerals in Soil Environments, 1989. **1**: p. 789-828.
31. Środoń, J., *Nature of mixed-layer clays and mechanisms of their formation and alteration.* Annual Review of Earth and Planetary Sciences, 1999. **27**(1): p. 19-53.
32. Zhang, C., et al., *Characteristics of clay-abundant shale formations: use of CO_2 for production enhancement.* Energies, 2017. **10**(11): p. 1887.

33. Kozeny, J., *Über kapillare leitung des wassers im boden:(aufstieg, versickerung u. Anwendung auf die bewässerg); gedr. Mit unterstütztg aus d. Jerome u. Margaret stonborsugh-fonds*. 1927: Hölder-Pichler-Tempsky, A.-G.[Abt.:] Akad. d. Wiss.
34. Shaw, H., *MJ Wilson, Ed. Clay Mineralogy: Spectroscopic and Chemical Determinative Methods. Chapman & Hall, London. 1994. 367 pp. Price£ 79.00. ISBN 0-412-533804*. Mineralogical Magazine. Vol. 58. 1994. 701-701.
35. Ma, Z., et al., *Review of application of molecular dynamic simulations in geological high-level radioactive waste disposal.* Applied Clay Science, 2019. **168**: p. 436-449.
36. Baptist, O.C. and S. Sweeney, *The effect of clays on the permeability of reservoir sands to waters of different saline contents.* Clays and Clay Minerals, 1954. **3**(1): p. 505-515.
37. Amorim, C., et al., *Effect of clay–water interactions on clay swelling by X-ray diffraction.* Nuclear Instruments and Methods in Physics Research Section A: Accelerators, Spectrometers, Detectors and Associated Equipment, 2007. **580**(1): p. 768-770.
38. Slade, P., J. Quirk, and K. Norrish, *Crystalline swelling of smectite samples in concentrated NaCl solutions in relation to layer charge.* Clays and Clay Minerals, 1991. **39**(3): p. 234-238.
39. Schad, S.T., *Hydrocarbon potential of the caney shale in southeasteastern oklahoma*. 2004, University of Tulsa.
40. Houseknecht, D.W., et al., *Assessment of undiscovered natural gas resources of the Arkoma basin province and geologically related areas*. 2010, US Geological Survey.
41. Kamann, P.J., *Surface-to-subsurface correlation and lithostratigraphic framework of the Caney Shale (including the" Mayes" Formation) in Atoka, Coal, Hughes, Johnston, Pittsburg, and Pontotoc Counties, Oklahoma*. 2006, Oklahoma State University.
42. Radonjic, M., et al. *Integrated microstructural characterisation of caney shale, ok*. in *Unconventional Resources Technology Conference, 20–22 July 2020*. 2020. Unconventional Resources Technology Conference (URTeC).
43. Nguyen, N.-T., S.T. Wereley, and S.A.M. Shaegh, *Fundamentals and applications of microfluidics*. 2019: Artech House.
44. Whitesides, G.M., *The origins and the future of microfluidics.* Nature, 2006. **442**(7101): p. 368-373.
45. Sohrabi, M., et al. *Visualization of oil recovery by water alternating gas (WAG) injection using high pressure micromodel-oil wet and mixed wet systems, SPE 71494*. in *SPE Annual Technical Conference and Exhibition, New Orleans, La*. 2001.
46. Gerami, A., et al., *Coal-on-a-chip: visualizing flow in coal fractures.* Energy & Fuels, 2017. **31**(10): p. 10393-10403.
47. Wang, W. and S. Chang. *Fabricating reservoir micromodels by in situ grown calcium carbonate nanocrystals in microfluidic channels*. in *Abstracts of Papers of The American Chemical Society*. 2017. AMERICAN CHEMICAL SOCIETY 1155 16TH ST, NW, WASHINGTON, DC 20036 USA.

48. Wang, G.C., *The utilization of slag in civil infrastructure construction*. 2016: Woodhead Publishing.
49. Zhang, Y., et al., *Geomaterial‐functionalized microfluidic devices using a universal surface modification approach.* Advanced Materials Interfaces, 2019. **6**(23): p. 1900995.
50. Guo, Y. and X. Yu, *Characterizing the surface charge of clay minerals with Atomic Force Microscope (AFM).* AIMS Materials Science, 2017. **4**(3): p. 582-593.
51. Kumar, N., et al., *Probing the surface charge on the basal planes of kaolinite particles with high-resolution atomic force microscopy.* Langmuir, 2017. **33**(50): p. 14226-14237.
52. Hoogenboom, B.W., *AFM in Liquids*, in *Encyclopedia of Nanotechnology*, B. Bhushan, Editor. 2012, Springer Netherlands: Dordrecht. p. 83-89.
53. Köster, H., *Mineralogical and chemical heterogeneity of three standard clay mineral samples.* Clay Minerals, 1996. **31**(3): p. 417-422.
54. Amscope. *40x-2500x led binocular compound microscope w 3d two-layer mechanical stage*. 2021 [cited 2021 05/31/2021]; Available from: https://www.amscope.com/compound-microscopes/brightfield/40x-2500x-led-binocular-compound-microscope-w-3d-two-layer-mechanical-stage.html#product_tabs_additional_tabbed.
55. Laboratory, O.S.U.M. *Equipment*. 2021 [cited 2021 05/31/21]; Available from: https://research.okstate.edu/microscopy/equipment/equipment.html.
56. Shaik, I.K., et al., *A parametric study of layer-by-layer deposition of $CaCO_3$ on glass surfaces towards fabricating carbonate reservoirs on microfluidic chips.* Journal of Petroleum Science and Engineering, 2020: p. 108231.
57. Tsai, W.-H., *Moment-preserving thresolding: A new approach.* Computer Vision, Graphics, and Image Processing, 1985. **29**(3): p. 377-393.
58. ImageJ Documentation Wiki, *Analyze Particles.* 2019.
59. Lebedeva, E.V. and A. Fogden, *Adhesion of oil to Kaolinite in water*. Environmental Science & Technology, 2010. **44**(24): p. 9470-9475.
60. El-Dessouky, H.T. and H.M. Ettouney, *Fundamentals of salt water desalination*. 2002: Elsevier.
61. Barhoum, A., et al., *Physicochemical characterization of nanomaterials: Polymorph, composition, wettability, and thermal stability*, in *Emerging Applications of Nanoparticles and Architecture Nanostructures*. 2018, Elsevier. p. 255-278.
62. Tang, G. and N.R. Morrow, *Salinity, temperature, oil composition, and oil recovery by waterflooding.* SPE Reservoir Engineering, 1997. **12**(04): p. 269-276.
63. Batias, J., et al. *Field and laboratory observations of Remaining oil saturations in a light oil reservoir flooded by a low salinity aquifer*. in *Paper SCA2009-01 presented at the 23rd International Symposium of The Society of Core Analysts, Noordwijk Aan Zee, The Netherlands*. 2009.

VITA

Rupom Bhattacherjee

Candidate for the Degree of

Master of Science

Thesis: PREPARATION OF CLAY-COATED GLASS SURFACES FOR MICROFLUIDICS-BASED STUDY ON CLAY-FLUID INTERACTIONS

Major Field: Petroleum Engineering

Biographical:

Education:

Completed the requirements for the Master of Science in Petroleum Engineering at Oklahoma State University, Stillwater, Oklahoma in July, 2021.

Completed the requirements for the Bachelor of Science in Petroleum and Mining Engineering at Shahjalal University of Science and Technology, Sylhet, Bangladesh in 2017.

Professional Memberships:

Society of Petroleum Engineers (SPE)